I.O.S.

THE DETAILED PROCESSES OF SEDIMENT TRANSPORT BY TIDAL CURRENTS AND BY SURFACE WAVES

R.L. SOULSBY, A.G. DAVIES & R.H. WILKINSON

REPORT NO. 152
1983

NATURAL ENVIRONMENT RESEARCH COUNCIL

INSTITUTE OF OCEANOGRAPHIC SCIENCES

INSTITUTE OF OCEANOGRAPHIC SCIENCES

Wormley, Godalming,
Surrey, GU8 5UB.
(0428 - 79 - 4141)

(Director: Dr. A.S. Laughton FRS)

Bidston Observatory,
Birkenhead,
Merseyside, L43 7RA.
(051 - 653 - 8633)

(Assistant Director: Dr. D.E. Cartwright)

Crossway,
Taunton,
Somerset, TA1 2DW.
(0823 - 86211)

(Assistant Director: M.J. Tucker)

When citing this document in a bibliography the reference should be given as follows:-

SOULSBY, R.L., DAVIES, A.G. & WILKINSON, R.H. 1983 The detailed processes of sediment transport by tidal currents and by surface waves.
Institute of Oceanographic Sciences, Report, No. 152, 80pp.

INSTITUTE OF OCEANOGRAPHIC SCIENCES

TAUNTON

The detailed processes of sediment transport by tidal currents and by surface waves

by

R.L. SOULSBY, A.G. DAVIES & R.H. WILKINSON.

I.O.S. Report No. 152

1983

This project was supported financially by the Department of the Environment

CONTENTS

ABSTRACT

This report summarises the main results obtained during a 3 year period of funding by the UK Department of the Environment on the subject of sand transport by waves and by currents. The aim of the project was to investigate and clarify those aspects of the application or interpretation of existing laboratory and river based sediment transport relations which lead to difficulties when they are used in the sea. Most of the work is based on field experiments, together with some supporting theoretical studies. The topics covered are: i) the form of the velocity, shear stress and turbulent energy profiles in the tidal bottom boundary layer; ii) the measurement and prediction of bed shear stresses and roughness lengths in the sea; iii) the effect of ripple dynamics and sediment transport on roughness lengths; iv) the structure of the Reynolds stress in terms of the bursting phenomenon; v) the correlation between bursting and sediment suspension; vi) density stratification effects due to suspended sediment; vii) direct measurement of the upwards diffusive flux of sediment; viii) the form of the near-bottom velocity profile under waves; ix) the determination of the threshold free stream velocity amplitude and threshold bed shear stress for sediment motion, beneath waves; x) the wavelength of ripples formed beneath waves; xi) the partitioning of the total bed shear stress between form drag and skin friction for wave motion over a rippled bed; xii) the critical condition for the onset of vortex formation and shedding above a rippled bed; xiii) the development of sensors to measure sediment transport as bedload and in suspension. Topics i) to vii) deal with tidal currents in the absence of waves, while topics viii) to xii) deal with wave motion in the absence of currents. Details of experimental and analytical methods are not included, but references to fuller papers covering the individual topics are given. Because this is a continuing programme of research, the analysis of some of the experiments performed is still underway, while some of the results presented stem from experiments performed before the start of the funding period. An appendix is included which gives a glossary of terms used in the report which may not be in common use in some branches of engineering.

1. INTRODUCTION

In many aspects of coastal management it is necessary to be able to predict the rate of erosion or deposition of sediment, both as it occurs naturally and as it might be modified by man's intervention. These include beach erosion, maintenance of dredged channels, estimating navigation depths, extraction of sand and gravel, and silting of basins. The sediment may move as bedload or in suspension, under the action of tidal currents or surface waves or a combination of both.

The essence of all these problems is prediction of the geographical distribution of bed level changes due to sedimentary processes. This can be forecast, subject to knowledge of local conditions such as grain size, water depth, current speed (or better, bed shear stress) and wave climate, using the sediment continuity equation together with an appropriate sediment transport formula. The former of these is fundamental and unequivocal, but the latter is generally an empirical or semi-empirical function of the input parameters.

A wide choice of sediment transport formulae is available to the engineer. All of them are based on river or laboratory studies however, and are generally not formulated to cope with the particular conditions prevailing in the sea. As an example of their unreliability in the sea,we may cite one of the few comparative tests conducted with marine data. Heathershaw (1981), using the same input data in five of the most widely accepted formulae (as part of the DoE funded study of Swansea Bay), found that their answers varied through a factor of 50. Furthermore, no one formula could be chosen as the most successful, as different formulae gave the best agreement with the measured transport rate at different sites.

The prediction of sediment transport due to surface waves also presents difficulties when applied in the sea because of the randomness of sea waves. Thus there is need for improvement in prediction techniques for both tidally induced and wave induced sediment transport. Aspects which have been identified as requiring attention are described at the heads of Section 2 (tidal currents) and Section 3 (waves).

The aim of this study is to further the understanding of the physical processes involved in some of these areas, and thereby to improve the prediction

capability. We consider only non-cohesive sediment, in particular sand, as the processes involved are then purely physical, and not biological or electrochemical. We have concentrated over the last 3 years on understanding sediment transport by currents and by waves separately. This is intended to lead up to a study of sediment transport by waves superimposed on a current, which is the case of greatest practical importance.

Although the present project has treated tidal currents and surface waves separately, the two topics have much in common. Both involve oscillatory flows and hence the boundary layer structures in the two cases have many common features. However, because of the difference in wave period of about three orders of magnitude between the two cases, gross differences in the scales of the respective boundary layers arise. While the wave boundary layer is a layer of intense shear only a few centimetres thick even when fully turbulent, tidal flow in coastal waters is often turbulent throughout the depth. Despite such differences, the two cases can be viewed as part of a single problem, as will be seen increasingly in the combined wave/current study.

This report gives a résumé of the principal results which have emerged from the study. Further descriptions of the experimental details and methods are presented in papers which either have been, or will be, published in the open literature. Some of the more recent results quoted herein are preliminary, and require further work before they are established rigorously enough for open publication. The programme is a continuing one, so some of the data analysed stems from experiments performed before the funding period, while some of the most recent experiments will continue to be analysed after the end of it.

2. SEDIMENT TRANSPORT BY TIDAL CURRENTS

2.1 Background

The following features of sediment transport by currents are among those which have been identified by users as causing difficulty in the application of prediction formulae in the sea:

i) The most critical input parameter is the bed shear stress τ_0. While it can be obtained from the water surface slope of a river, this is generally not

available in the sea, nor would it give a valid estimate of τ_0 if it were. The approach usually used is to obtain τ_0 from current measurements at one height, via either a quadratic friction law or, equivalently, the logarithmic velocity profile. The former requires knowledge of a drag coefficient and the latter a roughness length z_0. The specification of neither of these is well-established in the sea.

ii) Tidal currents are essentially oscillatory, whereas the formulae are designed for steady flow. The effect of acceleration on velocity profiles, concentration profiles and τ_0 has to be determined.

iii) A mobile sandy sea bed is generally rippled. The total bed shear stress as obtained from near bed velocity measurements is the sum of the skin friction and the form drag on the ripples. It is essentially only the skin friction which moves the sand grains, and so the partitioning of the total stress must be known. The methods differ for tidal and wave-induced flows.

iv) The bed shear stress varies spatially over both ripples and larger bedforms. Since the sediment transport rate is a highly non-linear function of τ_0, the spatially averaged sediment transport rate is not simply related to the spatially averaged τ_0.

v) The density gradients caused by suspended sediment may be sufficient to modify the turbulence characteristics, and hence the velocity and concentration profiles of the flow. The circumstances under which this is important, and the degree of turbulence damping, need to be established.

vi) While the shape of the suspended sediment concentration profile (for low concentration) is quite well established, the specification of the reference concentration which scales it is not. Thus there is uncertainty in quantifying the suspended sediment load. This is one of the least understood areas, and one of the greatest sources of error.

We have addressed those topics from the above list which were considered to be both important from the prediction point of view, and tractable in terms of the experimental and theoretical tools available to us. At the same time the topics have an intrinsic interest, in the wider scientific context.

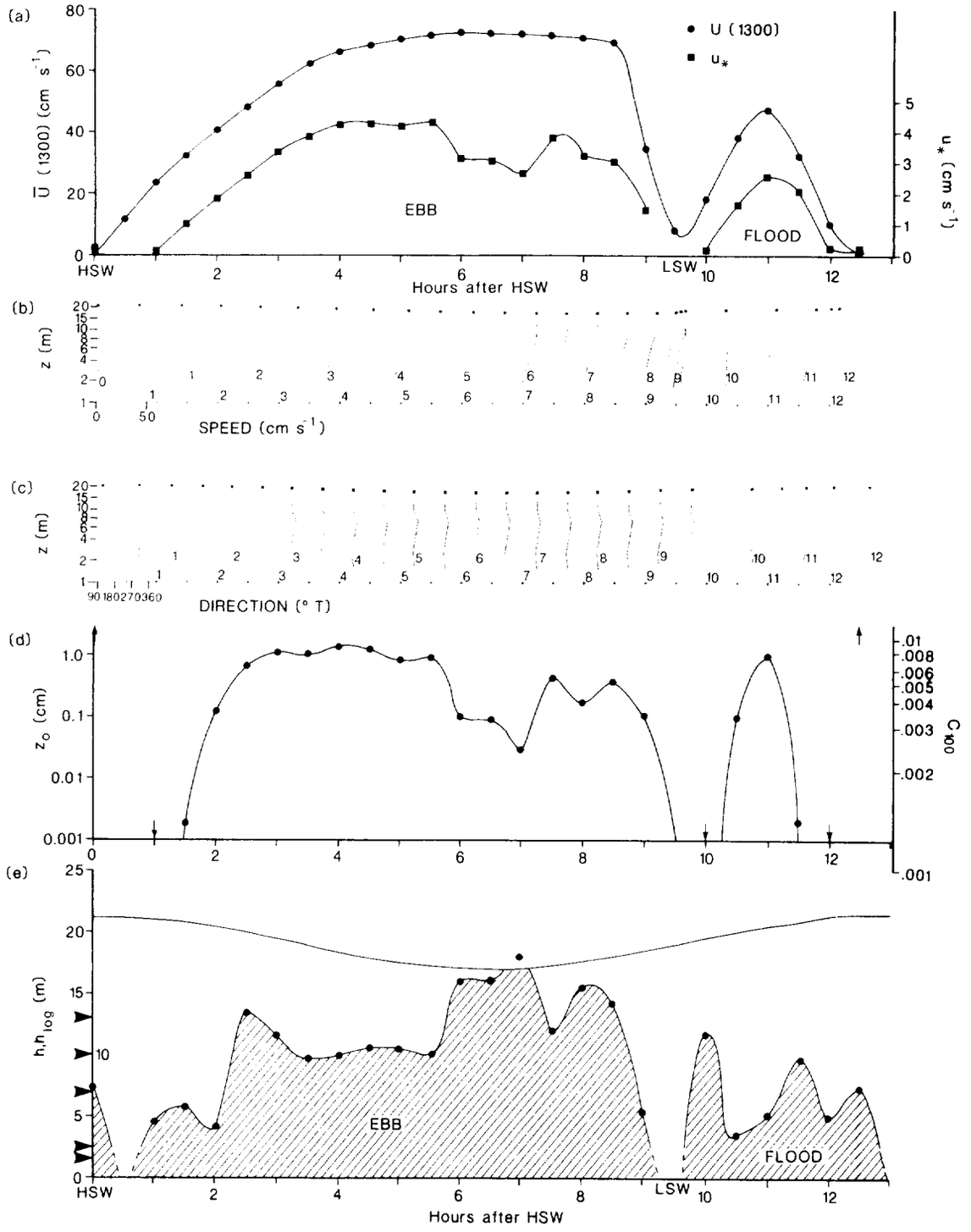

Fig 1: Flow parameters through an ensemble-average tidal cycle measured in Start Bay. (a) Current speed at 13 m above the bed, and the friction velocity u_*. (b) Vertical profiles of current speed averaged over half-hourly intervals. Crosses indicate the origin of the correspondingly numbered profile, and asterisks the water surface. (c) As for (b) but current directions. Crosses indicate 90° for the correspondingly numbered profile. (d) The roughness length z_o, and drag coefficient $C_{100} = \{0.4/\ln (100/z_o)\}^2$. (e) The water depth h, and height of the logarithmic layer h_{log} as defined in the text. Arrows against the h axis indicate the heights of the current meters.

2.2 Velocity profiles in the tidal bottom boundary layer

In order to study the effect of tidal oscillation on the estimation of τ_0 and z_0 (points i and ii above), a string of 6 current meters was deployed in a depth of 20 m in Start Bay, South Devon, from 2nd October to 11 October 1979. The aims were:

a) to study velocity and shear stress profiles through the depth in a nearly rectilinear flow, and
b) to provide background information for the more detailed near-bottom studies performed at a station 600 m to the east.

A more detailed description of the site is given in Soulsby (1983). Good data was obtained from 5 of the current meters for most of the period. Little variation from tide to tide was found in the velocity structure over a period of 4 days spanning spring tides, so 8 tidal cycles were ensemble-averaged to produce a representative semidiurnal tidal cycle with correspondingly less random fluctuation. The velocity profiles (Fig 1b), averaged over 30 min, show that vertical variation extends up to 13 m at least, and in all probability it extends right to the water surface. This shows that the tidal boundary layer is depth-limited here throughout the tidal cycle, so that its thickness is equal to the water depth. The form of the profile is more clearly established in the long ebb tide, flowing at almost constant direction (Fig 1c), which occurs at this site, than in the short variable flood tide. The current speed profiles, for the ebb tide only, are shown more clearly in Fig 2, with some of the half-hourly profiles omitted for clarity, and the decelerating profiles shown mirrored about the z axis. From 1 hour to 3.5 hours after high slack water (HSW), a midwater maximum appears in the profiles. This characteristic of accelerating velocity profiles is discussed by Soulsby and Dyer (1981) in the context of near-bed ($z < 2$ m) profiles, in which a theoretical form was presented for the velocity profiles with arbitrary acceleration/deceleration. During the central phase of the tide (4.5 to 7.5 hours after HSW) the velocity is proportional to $\ln z$, where z is the height above the bed, over a large fraction of the depth. From 8 to 9.5 hours after HSW the profile is concave downward, as is characteristic of decelerating profiles (Soulsby and Dyer 1981).

Values of the friction velocity $u_* \equiv (\tau_0/\rho)^{\frac{1}{2}}$ and roughness length z_0 were estimated by assuming that a logarithmic velocity profile passed through the meters at 1.5 m and 2.5 m (Figs 1a and 1d). The value of z_0 over the period 2.5

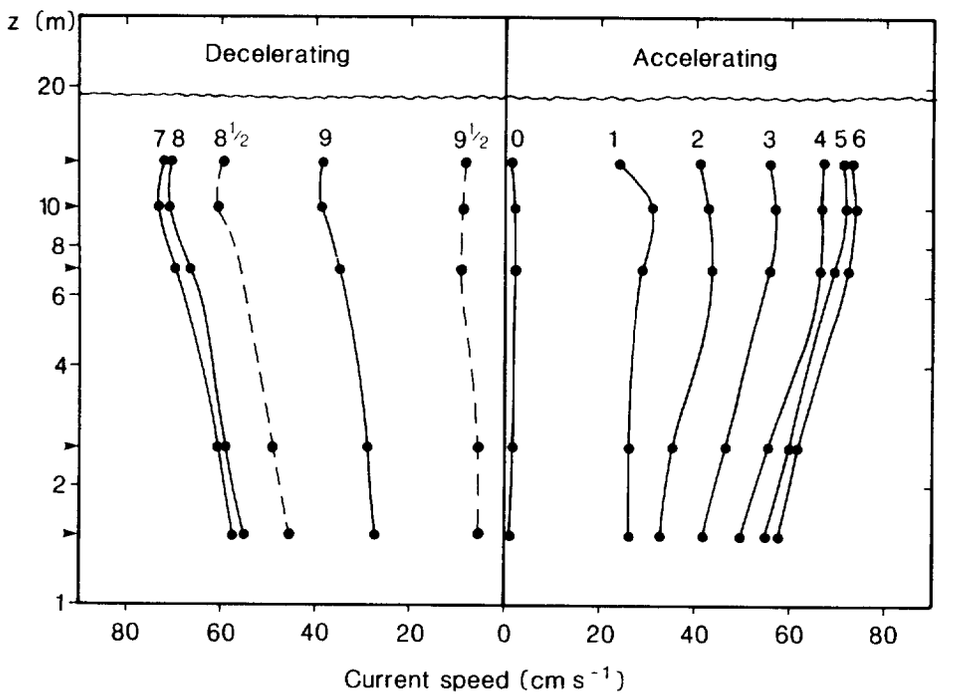

Fig 2: Current speed profiles averaged over half-hourly intervals in Start Bay. For clarity some of the profiles are omitted, and the decelerating profiles are plotted as a mirror image. Numbers against the profiles denote hours after HSW. Arrows against the ordinate indicate the heights of the current meters.

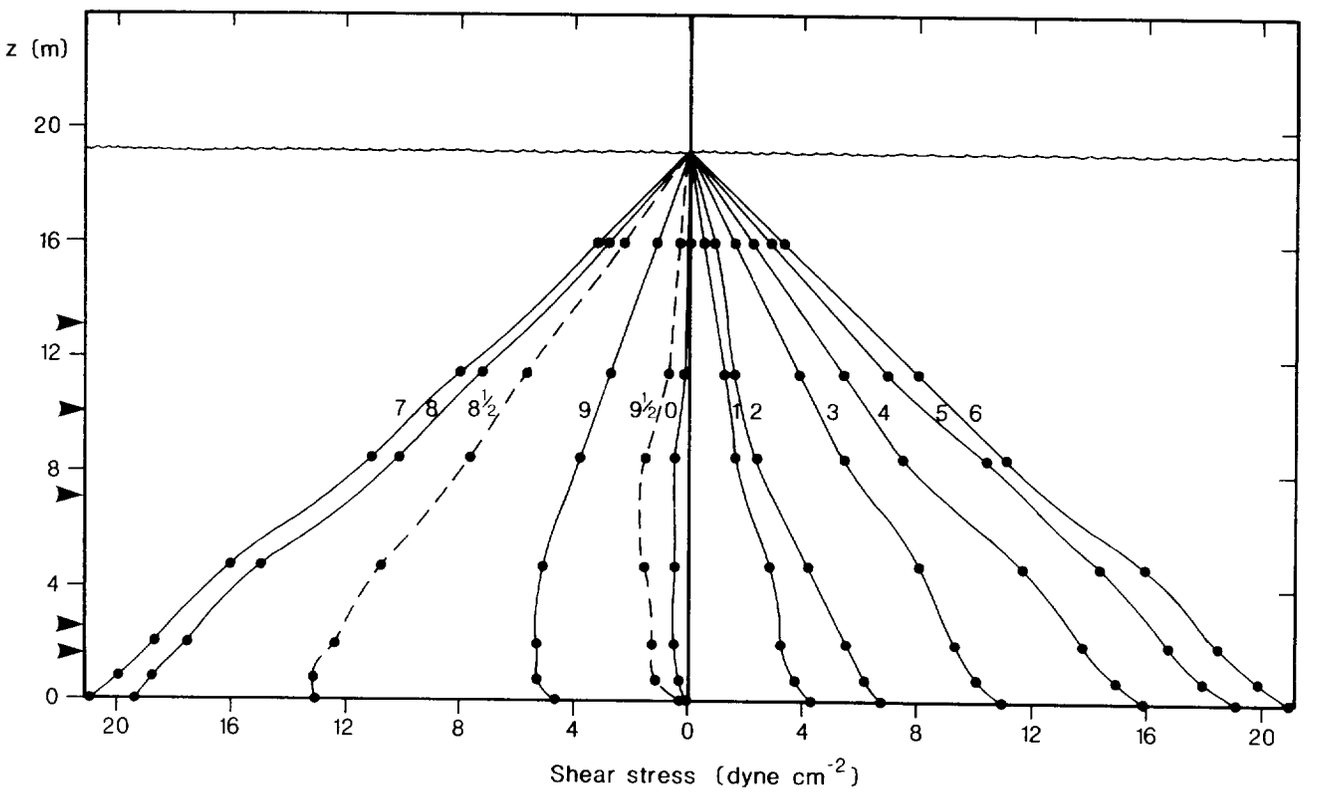

Fig 3: Profiles of the south-north component of shear stress averaged over half-hourly intervals in Start Bay. Same comments and symbols as in Fig 2.

to 5.5 hours after HSW is about 1 cm, which is a reasonable value for the rippled sand bed over which the measurements were made. In the periods extending 2 hours after HSW and 0.5 hours before LSW, z_0 varies widely, and it may be assumed that the logarithmic profile is not applicable then. The values of u_* at these times must also be suspect (Fig 1a). Over the period 6 to 7 hours after HSW, z_0 reduces to 0.03 cm, probably as a result of sediment transport occurring. The mechanisms causing this are investigated further in sections 2.4 and 2.7. The apparent value of u_* is also reduced during this period. During the short flood tide the value of z_0 only briefly attains 1 cm. A scale for the drag coefficient C_{100} referenced to the current at z = 100 cm is shown at the right hand side of the z_0 plot.

The height to which the velocity profile takes the logarithmic form varies through the tidal cycle (Fig 1e). We may define h_{log} as the height to which the measured profile fits the logarithmic form,passed through the meters at 1.5 m and 2.5 m,to better than ±5%. At 0.5 hours after HSW the velocity gradient was negative, so we must conclude that $h_{log} << 1.5$ m. Between 1 and 7 hours after HSW, h_{log} increased progressively until at 7 hours after HSW it reached the water surface. Although this includes the time when the profile may have been affected by sediment transport, it may nonetheless be a valid result, as we will see in section 2.7 that only the lower part of the profile (below 1.5 m) is affected by the density gradient, with the upper part remaining effectively logarithmic. From 7 hours after HSW, h_{log} decreased rapidly to a value << 1.5 m at LSW. During the short flood tide, h_{log} does not have time to increase beyond 10 m before falling back to a small value at 0.5 hours after HSW.

The use of the logarithmic profile (or equivalently the quadratic friction law) to predict τ_0 and z_0 is thus not valid at times in the vicinity of slack water. We might as a general rule suggest that the period one hour before, to one hour after, slack water be excluded. More specifically, the height to which current measurements are within the logarithmic region increases as the tide runs, to reach a maximum which may correspond with the water surface. It then decreases as slack water is approached. The contentious times are thus those which are likely to be of least interest for coarse sediment transport. However, once sediment is in motion the values of τ_0 and z_0 obtained by this method are again questionable due to modification of the velocity profile.

The tidal variation in vertical profiles of the shear stress has also been calculated from the data (Fig 3). The method was identical with that used by Bowden et al (1959) for their measurements in Red Wharf Bay, North Wales. The present profiles show less structure than those of Bowden, in that the departure of the Start Bay profiles from a linear decrease in shear stress with height is less than that of the Red Wharf Bay profiles. The reason for this appears to be that the bed is much rougher in the Start Bay case ($C_{100} \cong 0.0075$, as compared with 0.0035 in Red Wharf Bay). The ratio of inertia to friction is thus smaller, and hence the departure from the quasi-steady linear height dependence is less.

The only profiles which show marked departures from the linear form are those from 0 to 2 hours after HSW, and those from 8.5 to 9.5 hours after HSW (ie within about 1.5 hours of LSW). The former show the concave upwards form of accelerating shear stress profiles, and the latter the midwater maximum stress which is characteristic of decelerating profiles. Again, the implication is that, in shallow flow over a rippled sand bottom, accelerative effects are only important during the hour or two either side of slack water, when movement of coarse sediment is least significant.

2.3 Turbulence profiles in the tidal bottom boundary layer

Having studied the tidal variation of the profiles of mean current velocity and shear stress, we now examine the tidal variation of profiles of turbulent kinetic energy. This affects the tidal dynamics through the shear stress, and also governs the suspension of sediment.

An exploratory experiment to measure profiles of turbulent kinetic energy repeatedly through a tidal cycle was made from an anchored ship in October 1981. It was made at the same station as the velocity profiles in section 2.2, to interrelate with them. Apart from the intrinsic scientific interest of these measurements, they will help to validate a theoretical model of the oscillatory boundary layer (applicable to either tidal or wave frequencies) which is being developed as an integral part of these studies. The technique proved successful and a first data set was obtained, though this was of poor quality because of bad weather. The analysis of it is still at an early stage. Spectra of the turbulent velocity components have been obtained (Fig 4), which show that although the vertical velocity component was dominated by the heave motion of the frame (which was measured with an accelerometer), the two horizontal components were not much

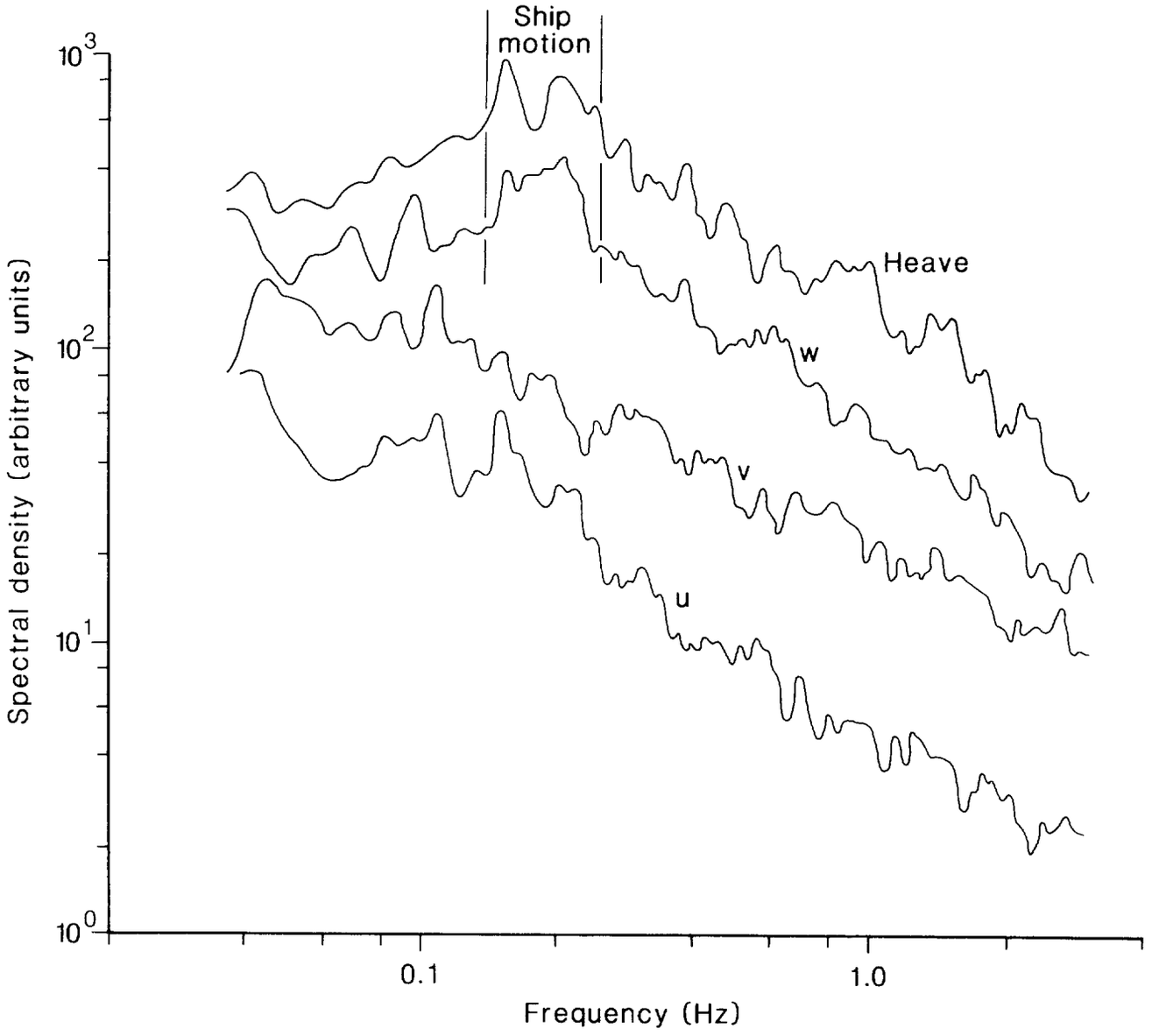

Fig 4: Energy spectra of the u, v and w components of velocity, and the heave velocity of the instrument frame, measured 6.8 m above the bed in water 21 m deep. The ship's roll period was about 4-7s.

affected. It is not yet known whether the measured heave can be successfully removed, but this should certainly be possible with future data sets made in calm weather.

2.4 Tidal variation of roughness length

The roughness length (z_0) of the seabed has been found by several workers to vary throughout a tidal cycle. This could be due to 3 effects, (i) the drag coefficient is not Reynolds number independent (ii) the roughness length is a function of the geometrical shape of the bed (eg Lettau, 1969) and this may vary during periods of the tide when sediment is in motion or (iii) the presence of a layer of moving sediment near the bed (eg Owen, 1964). Dyer (1980) measured large variations of 0.01 cm < z_0 < 5 cm above a rippled mobile sand bed, and proposed an explanation in terms of the above mechanisms. Fig 1d of this report also shows a slightly smaller, though still appreciable, variation. If z_0 does vary as the dimensions of the roughness element,as suggested by the literature, these changes need further investigation, as it is unlikely that the dimensions of the ripples change by an order of magnitude.

An experiment was performed in October 1981 when a frame (see Fig 5) equipped with propeller current meters, a camera and an optical device for ripple shape measurement, and a nozzle for pump sampling the suspended sediment was lowered onto a mobile rippled sand bed from a 3 point anchored ship. Six current meters were arranged at approximately logarithmic spacing in the bottom 2 m in order to measure the mean (10 min) velocity profile. This was used to calculate z_0 and u_* via a method that accounted for the unsteady nature of the flow (Soulsby and Dyer, 1981). The suspended sediment was repeatedly sampled during the experiment, and hence the concentration and grain size characteristics of the suspended load found. A grab sample of the bottom sediments was also obtained and analysed. The shape of the ripples immediately in front of the frame was recorded by photographing the shadow cast obliquely by a straight rod onto the seabed (Figs 5 and 6). Vertical sections through the ripples were calculated from the shape of the shadow and the known geometry of the camera/light/rod configuration (Wilkinson et al, 1983).

Velocity profiles and sediment samples were obtained for the duration of an ebb and a flood on 3 consecutive nights at spring tides, but equipment failure resulted in photographs of the bed only being acquired on the last night.

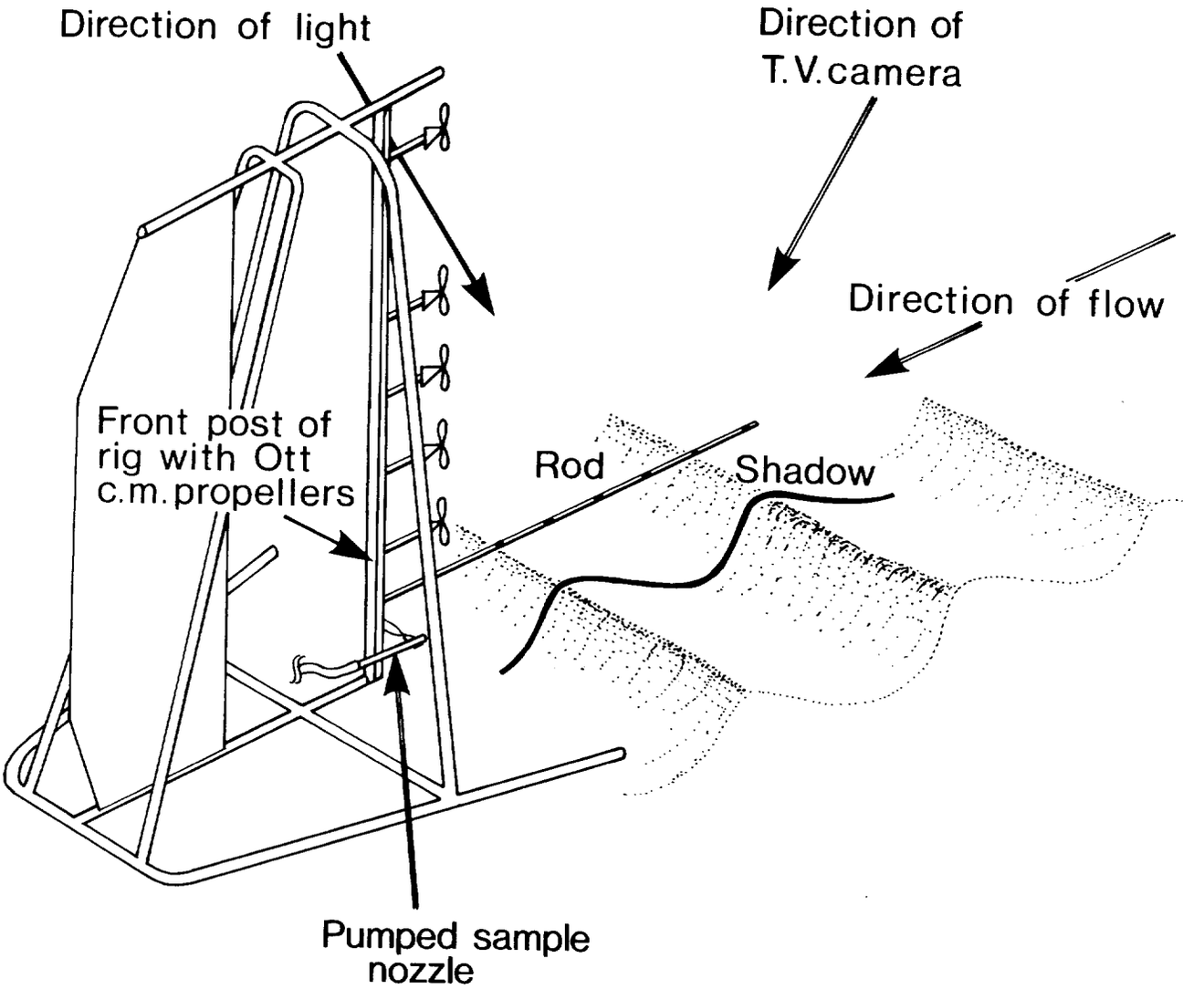

Fig 5: Experimental frame used for investigation of variation of u_* and z_o with ripple shape and suspended sediment transport

Fig 6: Example of photograph of ripple shape. Two rods were used in order to estimate the 3-dimensional nature of bed.

The values obtained for z_0 over a mobile rippled sand bed during this experiment were much less variable than those found by other workers. The consistent trend found on the 3 nights was for z_0 to increase gently through the duration of the ebb tide from a value of about 0.5 cm to about 1.3 cm (eg Fig 7). The variability of both u_* and z_0 about the trend line can be attributed to statistical scatter (Wilkinson, 1983). The extreme values of z_0 outside this range found by Dyer (1980), and in Fig 1d, tend to be at the beginning and end of the ebb, ie at times of the most rapidly changing velocity. In fact, even the gentle increase in z_0 found in all these experiments might be attributable to incomplete removal of acceleration and deceleration effects. There is no evidence of a dependence of z_0 on U_{100}, ie the drag coefficient C_{100} appears to be independent of Reynolds number ($= 100U_{100}/\nu$).

Owen (1964), working on aeolian sediment transport, proposed a dependence of z_0 on u_* associated with saltation of the sand grains. The hypothesis was modified for the sea by Smith and McLean (1977) and discussed by Dyer (1980). However, from the present results, there is no evidence of any relationship between z_0 and u_*, as u_* rises and falls whilst z gently rises (Fig 7). This may be because saltation is not an important mode of transport in aqueous flows.

The ripple photographs taken during an ebb tide showed that the bed becomes gradually more chaotic (ie less ripple-like) as the tide progresses. The dimensions and shape of the ripples were assessed by the wavelength (average of zero up crossing, peak to peak, and trough to trough), the amplitude and std dev of bed elevation and the skewness of the slope (Fig 8). None of these statistics were well behaved, displaying a large amount of scatter, probably as a result of the short sample length (about 4 wave lengths - Fig 6). The wavelength of the ripples showed a trend rising from 17 to 25 cm at peak flow, and returning to a value more like 15 cm. During this time, the height of the ripples showed little organised variation, remaining at about 0.7 cm std dev and 2.0 cm peak to trough amplitude, but with considerable scatter. The tidal conditions at the experimental site were such that the ebb and flood tides flow in practically opposite directions, with the ebb being dominant. Dyer (1980) reported observing that the direction of asymmetry of the ripples changed as the ebb flow developed, and attributed to it some of the large changes in z_o that he observed. A similar asymmetry was detectable in these results at the beginning of the ebb, ie the slightly gentler slope faced downstream. As the ripples became more chaotic, the

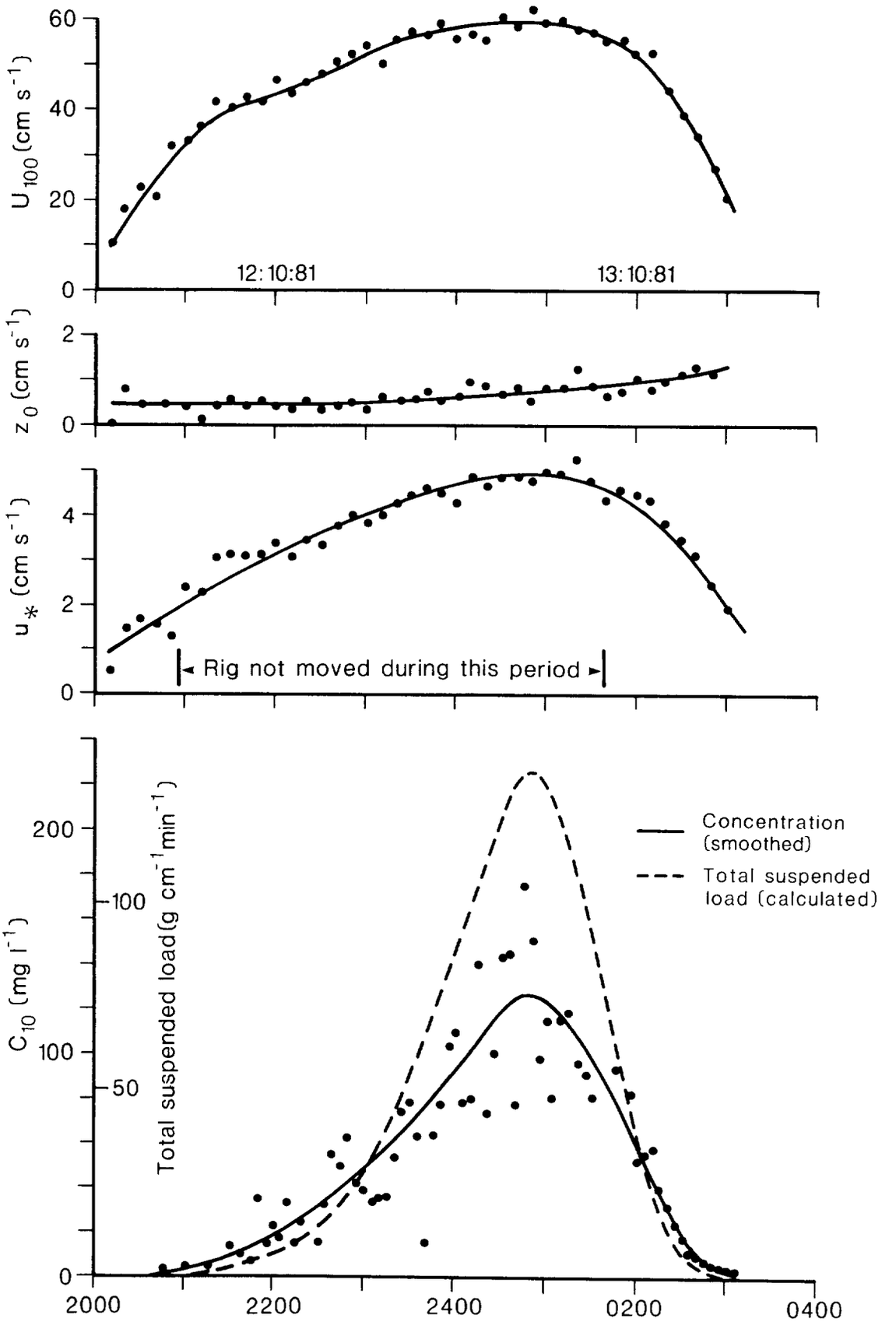

Fig 7: Typical behaviour of flow and sediment transport during an ebb tide.

asymmetry became undetectable. Attempts at quantifying this behaviour using the skewness of the slope as a measure of asymmetry were not satisfactory.

Lettau (1969) proposed the relationship $z_0 = H_R s/S$, where H_R is the obstacle height and s is the cross sectional area seen by the flow per horizontal area S. For ripples, s/S can be interpreted as the steepness, and so this formulation predicts that z_0 should vary from 0.12 cm to 0.08 cm and back to 0.13 cm as the ripple wavelength changes. This is not at all similar to the actual behaviour of z_0, but it is perhaps surprising that this method even gets the order of magnitude right, as it was originally proposed for roughness consisting of individual obstacles standing on a flat surface rather than a wavy surface itself.

The changes in shape of the bed are the result of sediment transport. More precisely, they are the result of local changes in sediment transport rate, ie erosion and deposition. These take place in a fairly orderly fashion, so that the bedform slowly moves downstream. It can be shown that the movement of material represented by the volume transport rate of the bedforms gives a lower bound to the actual sediment transport rate. The "bedform transport rate" was estimated viatwo routes, (i) a speed of propagation of the bedforms was obtained by lagged cross-correlation between consecutive ripple shapes and this was multiplied by the volume of the bedform and (ii) the rises and falls of the bed level between two records were summed separately to find the total increases and decreases in transport rate over the profile. As the transport rate must fluctuate with the same spatial frequency as the bed and cannot go negative (ie must be in the direction of flow), the minimum transport rate can be found. The speed of propagation of the ripples (when it could be measured - the ripples must be recognisable between photographs) varied smoothly with U_{100}, reaching a maximum of about 1.8 cm min^{-1} at maximum flow. For the size of ripples found here, this gives a maximum bedform transport rate of 2.5 gm $cm^{-1} min^{-1}$. The measurements of changes in bed level resulted in an estimated bedform transport rate of 2.1 gm $cm^{-1} min^{-1}$.

The suspended sediment samples that were obtained during the experiment showed that, as expected, the concentration at 10 cm above the bed varied smoothly during the tide reaching a maximum at the time of the most vigorous flow (Fig 7). A threshold shear velocity of about 1.9 cm s^{-1} was found for suspension of the sand ($d_{50} \cong 150\mu m$), above which the concentration was proportional to $u_*^{4.5}$. As the

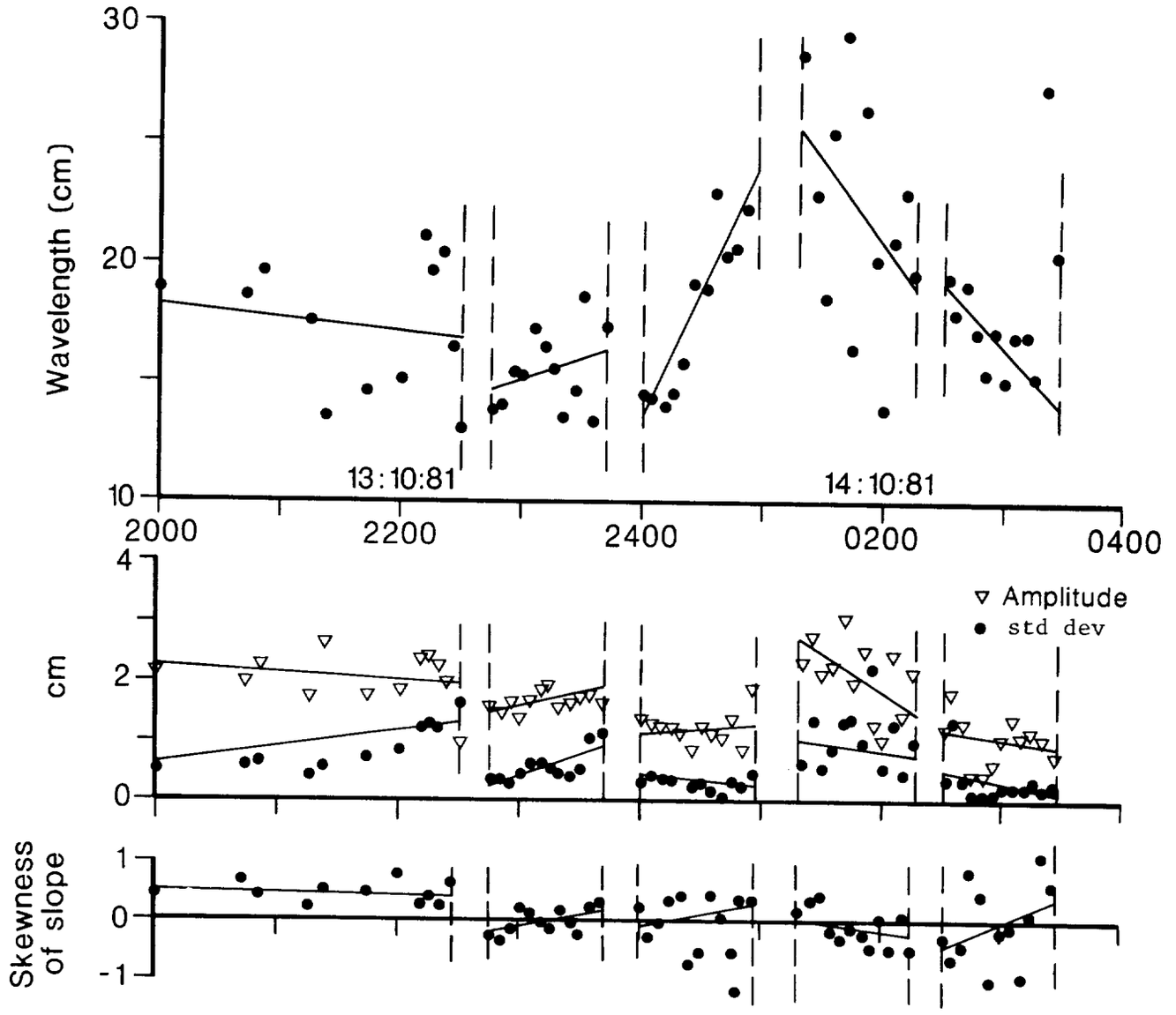

Fig 8: Behaviour of ripple statistics during an ebb tide.
(Gaps in the data are due to the frame being moved)

samples were obtained only at one height (10 cm) the shape of the concentration profile could not be compared with theory,but a Rouse(see Graf, 1971) profile was used to calculate a value of concentration at height z_o above the bed, and this was compared with an equation suggested by Smith and McLean (1977)

$$C(z_o) = \gamma\left(\frac{\tau - \tau_c}{\tau_c}\right)$$

where τ_c is the bed shear stress at the threshold of motion and γ is an empirical constant. Smith and McLean calculated this to be of the order of 10^{-3}, the exact value depending on the details of the computation. Assuming the relevant value of z_0 to be that found empirically, the present results give a value for γ of 0.84×10^{-4}, which agrees well with Dyer's value (found by the same method) of 0.79×10^{-4}. However, much the same value as that found by Smith and McLean is obtained if the relevant roughness is assumed to be the Nikuradse grain roughness as modified by bedload movement after the fashion of Owen (1964).

The assumed Rouse concentration profile was then combined with a logarithmic velocity profile after the fashion of Einstein (see Graf, 1971), but using the approximations of Soulsby (1978), and an example of the behaviour of the total suspended sediment load is given in Fig 7. The amount of bedload transport was estimated by the method of Bagnold (1980), and the quantities of sediment transport by various modes compared as follows. At peak flow, the total suspended load transport rate is about 130 gm $cm^{-1} min^{-1}$, whereas the bedload transport rate is only about 3 gm $cm^{-1} min^{-1}$. The latter is similar to the bedform transport rate, and it is reasonable to suppose that these two are closely associated, with the suspended load passing straight over the top, playing little part in ripple migration.

Suspension of sediment in the water column creates a vertical density gradient, which may cause the velocity profile to deviate from the usual logarithmic form. This can give apparent variations in z_0 in addition to any caused by the Owen (1964) mechanism. However, comparison of the behaviour of z_0 and concentration of suspended sediment throughout a tidal cycle in the present data reveals no correlation. The trend of z_0 is to rise gently, but the concentration has a peak at maximum flow, when sediment transport was very vigorous for maritime

conditions. Thus it can be concluded that although there was a considerable amount of sediment in suspension, it did not appear to modify the velocity profile. A possible reason for this is given in section 4.

2.5 The structure of the Reynolds stress

In a turbulent shear flow, such as that of the tidal current over the seabed, the friction between adjacent layers is carried by the Reynolds shear stress $\tau = -\rho\overline{uw}$. Here ρ is the water density, u and w are the horizontal and vertical fluctuating components of the water velocity, and the overbar indicates a mean over a time interval of order 10 mins. Measurement of the Reynolds stress provides an alternative means of estimating τ_0 for sediment transport, as in a simple flow $\tau_0 \cong \tau$ in a layer near the bed. In order to better understand the momentum transfer processes which go to make up the mean stress, it is helpful to examine the instant by instant contributions to the uw product (the density ρ is merely an effectively constant multiplying factor).

Laboratory experiments reported in the literature (Grass, 1971; Comte-Bellot et al, 1978), have shown that $\overline{uw}$ is made up of intermittent large contributions from short-lived events, separated by relatively quiescent periods. These have been shown by ourselves and others (Gordon, 1974; Heathershaw, 1974), to occur also in the sea, and an example from our measurements is shown in Fig 9. The events, taken to be those which make up 90% of the total $\overline{uw}$ (in descending order of $|uw|$ in the record), take instantaneous values of up to about 20 times the mean $\overline{uw}$, but have durations of less than about 5 s. The 86 events shown in Fig 9 accounted for 90% of the stress in only 26% of the time. They are classified by convention into 4 types according to the signs of u and w (see Fig 9). Most of the stress is generated by bursts ($u < 0$, $w > 0$) and sweeps ($u > 0$, $w < 0$). If the bed shear stress is similarly intermittent (and this remains to be shown), then the entrainment of sediment is likely to be dominated by these events. Our TV observations of the seabed show that at current speeds just above the threshold of motion, the sand is swept up from the bed in sporadic swirls, typically 50 cm across and a few seconds in duration. This is confirmed by measurements of the suspended sediment concentration made with the sand transport probe - see section 2.11. Independent laboratory evidence also indicates that sediment is carried into suspension in burst-like motions (Grass, 1974).

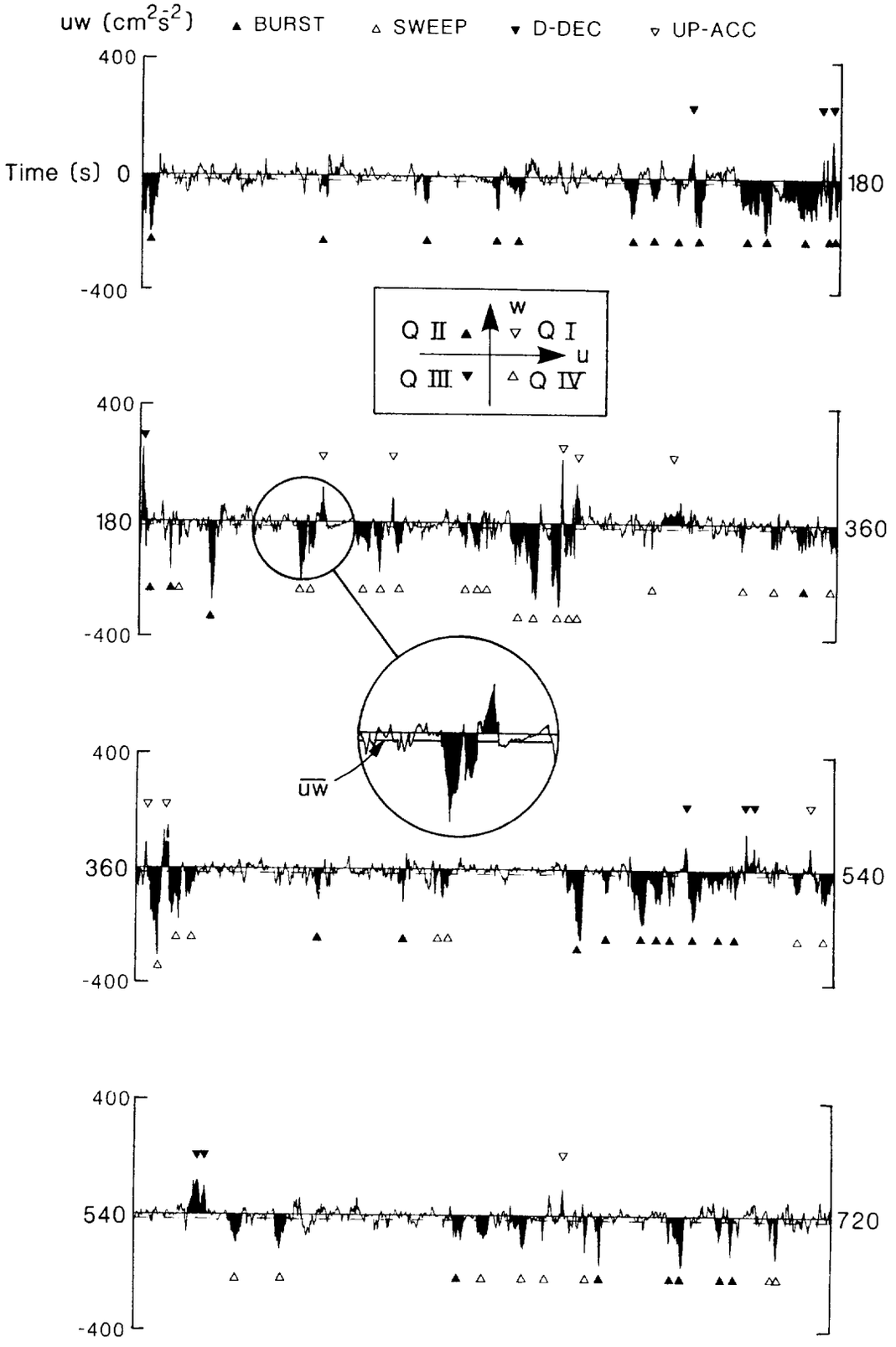

Fig 9: An example of the uw product for a 12 min record taken in Start Bay at a height of 140 cm. The 85 events which make up 90% of $\overline{uw}$ are shaded black and classified by quadrant. For this record $\bar{U}(140)$ = 51.3 cm s^{-1} and $-\overline{uw}$ (140) = 15.7 cm^2s^{-2}. A definition sketch for the 4 types of event and the 4 quadrants is given at the top of the figure.

Previous laboratory and marine investigators have concentrated on examining the structure and growth of the intermittent events. In the present study we have extended this by seeking to explain some of the well-known characteristics of the shear stress τ in terms of the intermittent events. Thus, for example, τ is known to vary as the square of the velocity (the quadratic friction law); but does this happen because there are more events, or longer-lasting events, or larger amplitude events, or fewer counterproductive events (ie up-accs and d-decs, see Fig 9) at faster current speeds? Figure 10 shows how all these properties vary, as the current speed at a station in Start Bay drops from its maximum flood tide value to slack water. A decrease in the number of events is offset by an increase in their duration; when converted to spatial scales this corresponds to the spacing between events, and their size, remaining roughly constant. The stress contribution from each kind of event also remains roughly constant, apart from an increase in all of them near to slack water as surface wave motions become prominent. However, the amplitude (defined as the mean $|uw|$ through an event) varies strongly, approximately as the square of the near surface velocity, and is deduced to be the mechanism underlying the quadratic friction law.

A similar comparison between a smooth bed of sandy gravel in Weymouth Bay (z_0 = 0.04 cm) and a rough bed of rippled sand in Start Bay (z_0 = 0.35 cm), showed little difference either in the spacing between events, or in their size. The contribution from counter-productive events was a little greater over the rougher bed, but this was greatly outweighed by an increase in the amplitude of the events over the rougher bed. Thus the underlying cause of the greater τ observed over rough than over smooth beds, for the same velocity,is principally the larger amplitude events caused thereby.

Further insight into the evolution of turbulent eddies, which may possibly be carrying sediment, can be gained from a study of the angle of their motion relative to the bed. This is obtained from the mean horizontal and vertical velocities during the event. It can be defined either as an absolute value, as would be seen by an observer standing on the seabed, or as a relative value, as would be seen by an observer travelling with the mean velocity at the measuring height. Taking 0° to be aligned downstream, and positive angles upwards, the absolute angle of motion of bursts was in the range 6° to 12° for the data sets described above, while that of sweeps was -5° to -8°. The relative angle of motion of bursts was 150° to 155° and of sweeps was -25° to -30°. In the

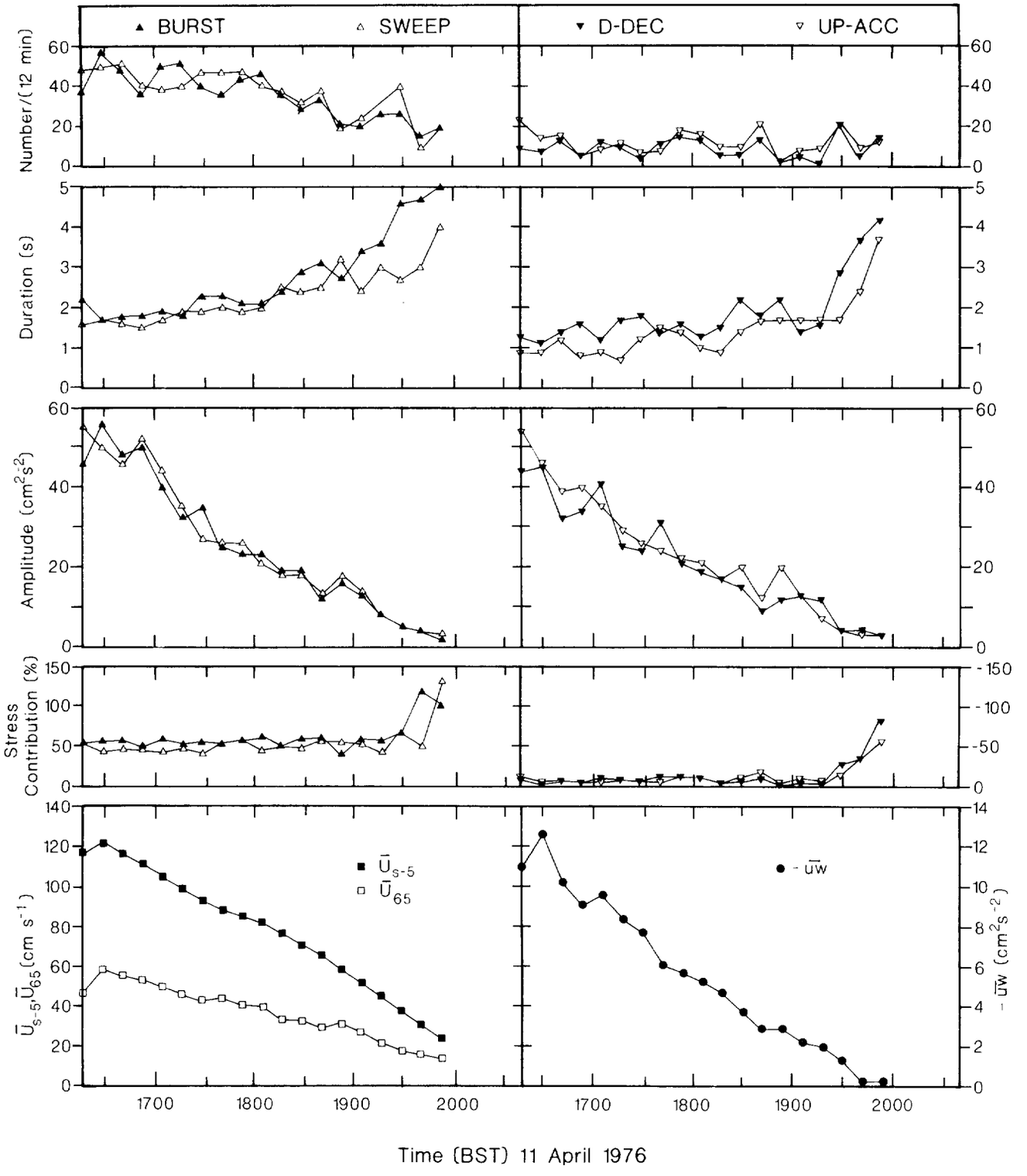

Fig 10: 12 min mean values of the number, duration, amplitude and stress contribution of the four kinds of bursting event. The measurements were made 65 cm above the sea bed in Start Bay, as the current decreased from its peak value to slack water. The water depth was 42 m, and the current speed $\bar{U}_{s-5}$ measured 5 m below the surface is shown, as well as the current speed $\bar{U}_{65}$ and kinematic shear stress $-\overline{uw}$ at the measuring height.

laboratory experiment of Grass (1974), sand grains were observed to be suspended by burst-like motions whose relative angle of motion varied from 130° near the bed to about 170° in the outer half of the boundary layer. The motion of sand grains will be directed at a lower angle than that of the water, because of settling.

More details of this work are given by Soulsby (1983). A full account, including sensitivity tests of the criterion for identifying events, a comparison with published pipe flow data on bursting, and presentation of additional features of the events, will also be written.

2.6 The flux-angle distribution

Further insight can be gained by examining the flux-angle distribution, used by micrometeorologists (eg McBean, 1974). This shows the proportion of the total $\overline{uw}$ which corresponds to air (or water) moving at a particular angle to the horizontal. The division into types of event is broadened to include all motions in each quadrant of u-w space (see Fig 9). Atmospheric flux-angle distributions are given in terms of 'updraughts', comprising up-accs (Quadrant I) and bursts (QII), and 'downdraughts', comprising d-decs (QIII) and sweeps (QIV).

An example from our marine data is shown as the heavy line in Fig 11, and reproduces the features observed in atmospheric distributions. For this case, positive contributions to $\overline{uw}$ are produced by updraughts at angles greater than 7°, and downdraughts between -16° and 0°. A region of negative contributions at small updraught angles (0° to 6° in our case) had been noted previously by meteorologists. When the distribution is subdivided into quadrants (the fine lines in Fig 11) it is immediately seen that most of $\overline{uw}$ results from motions in QII and QIV. However, the negative contribution in QI is larger than the positive in QII for small angles, giving rise to the previously noted behaviour. A slightly negative region for downdraughts steeper than -16° is similarly caused by QIII outweighing QIV here.

A paper is to be written describing the variation of both the absolute and relative flux-angle distributions with velocity, height and bed roughness.

2.7 A criterion for the degree of stratification caused by suspended sediment

It is well known that under some circumstances suspended sediment can cause

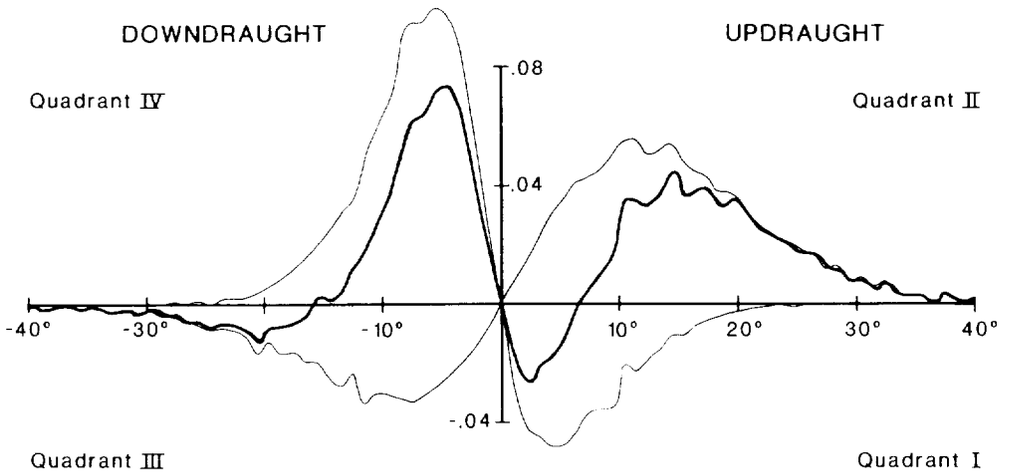

Fig 11: The flux-angle distribution for a four-hour period of steady current at a height of 30 cm above the bed in Start Bay. The heavy line shows the updraught-downdraught distribution, and the fine lines show the distribution divided into quadrants in the u-w plane (see Fig 9). Angles are relative to a stationary observer, with 0° downstream and positive upwards.

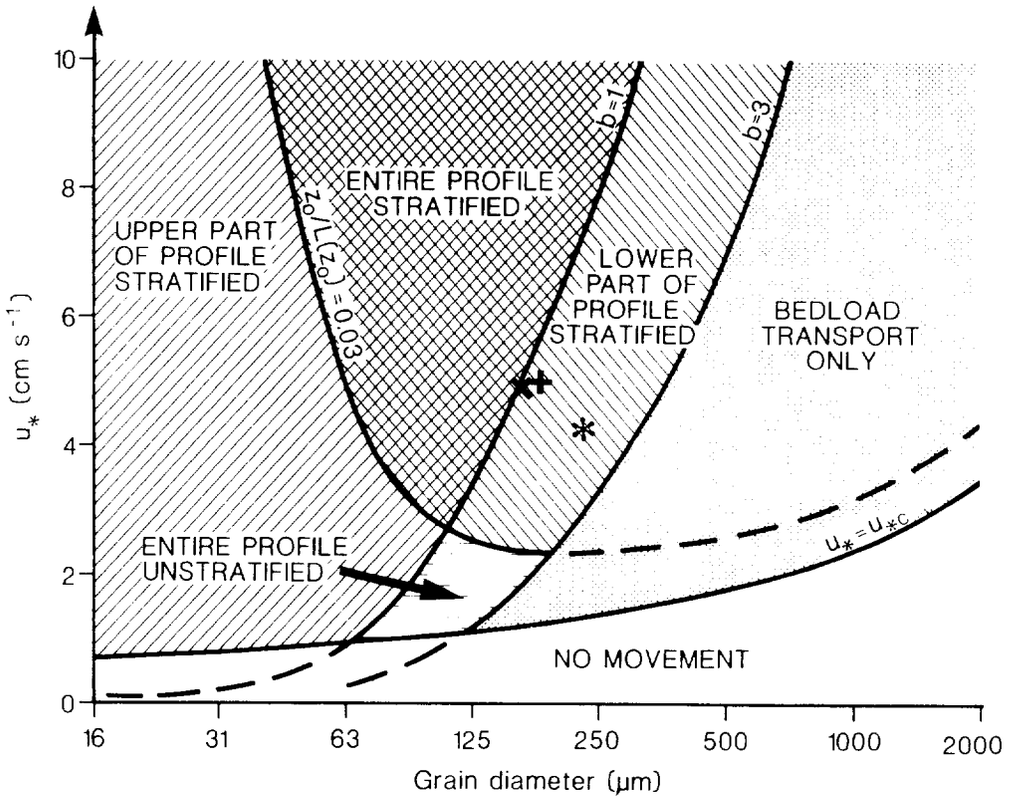

Fig 12: The gravitational stability of the water column when sediment is in suspension, as a theoretical function of the friction velocity u_* and grain diameter d. The values of u_* and d_{50} at the time of peak current for 3 field experiments are shown as follows:

* Start Bay current meter profiles (section 2.2), d_{50} from bed sample
+ Start Bay ripple experiment (section 2.4), d_{50} from suspended sample
× Taw experiment (section 2.9), d_{50} from suspended sample

sufficient density stratification of the water column as to modify the velocity profile from its usual logarithmic form. In the atmosphere, where vertical gradients of temperature have a similar effect, the criterion for the modification being appreciable is that $|z/L| > 0.03$. The Monin-Obukhov length L contains the ratio of the (shear stress)$^{3/2}$ to the density flux, and as both these are roughly constant in the lower part of the atmosphere, L is also constant. This is not true for the present case, as the density flux due to the sediment decreases strongly with height. Thus part of the profile may be stably stratified, and part near-neutral. Moreover, the density flux increases with the shear stress, so that it is not known at the outset whether an increase in shear stress will increase or decrease the stability parameter z/L.

To investigate this we have constructed a theoretical expression for z/L based on existing expressions for the suspended sediment concentration profile. For a deep, steady, uniform flow over a flat, unrippled bed of non-cohesive sediment, z/L can be written in terms of the height z, the friction velocity u_*, the threshold shear stress ρu^2_{*c} for bedload transport, and the settling velocity w_s of the grains. The latter two can be obtained from known empirical functions of the grain diameter d. Thus assuming quartz grains in water at 20°C, the stability can be calculated as a function of z, d and u_* only.

It transpires that the height dependence of z/L is such that if $b \equiv w_s/\kappa u_* > 1$, then z/L decreases with z, but if $b < 1$, then z/L increases with z. Here κ is von Karman's constant, whose value derived from our marine measurements is 0.40 (Soulsby and Dyer 1981). Thus if the top of the bedload layer is at $z = z_o$, then if $z_o/L(z_o) > 0.03$ and $b < 1$, the entire water column is stably stratified, but if $b > 1$, a height will be reached at which $z/L = 0.03$ and above this the water column is near-neutral. If $z_o/L(z_o) < 0.03$ and $b > 1$, the entire water column is near-neutral, but if $b < 1$, a height will be reached at which $z/L = 0.03$ and above this the water column is stably stratified. The curve $z_o/L(z_o) = 0.03$, as a function of u_* and d, is plotted in Fig 12, together with the curve $b = 1$, and curves delineating the thresholds of bedload and suspended transport. Figure 12 indicates at a glance whether or not suspended sediment will cause significant stratification of the water column, for a particular u_* and d. A paper giving the full theoretical treatment is to be written.

2.8 The Sand Transport Probe

An essential part of the project was the development of a sensor to measure the concentration of sand-sized particles in suspension in tidal flows. The aim was to produce an instrument whose frequency response was sufficient to allow the turbulence characteristics of the concentration field to be determined, and when taken together with simultaneous turbulent velocity measurements, to permit the flux of sediment to be calculated. Optical devices, which are satisfactory for silt-sized particles are less suitable for sand, as a small concentration of suspended mud can obscure a much larger concentration of sand.

The original sensor consisted of a 6 mm diameter disc of piezo-electric ceramic mounted in the flow so that the suspended sand grains struck its front face, each impact being converted by the ceramic to a voltage pulse. The sand concentration can then be derived from the impact rate and the independently measured water velocity. In addition, the height of the voltage pulse is proportional to the momentum of the grain so that a crude grain size distribution can be obtained by pulse height discrimination. A useful feature of the behaviour of grains carried by a fluid around an obstacle is that when the Stokes number (a dimensionless group which combines the grain size and density, water velocity and viscosity, and obstacle size) falls below a critical value, the grain does not strike the obstacle. This means that the sensor can be designed to discriminate against silt and clay grains smaller than a chosen size.

Field tests were performed on a prototype impact sensor, in which it was mounted 23 cm above the sea bed in a tidal current in Start Bay, with a nozzle mounted adjacent to it through which pumped samples were taken. Mean concentrations derived from the impact sensor correlated well with those obtained from the simultaneous pumped samples over the concentration range 3 mg l^{-1} to 50 mg l^{-1}, occurring at the site (Fig 13). Grains in the size range 40 μm to 800 μm were in suspension, and sieving of the pumped samples showed that the minimum diameter to which the sensor responded was 110 μm. This compared with a theoretical value of 90 μm derived from the critical Stokes number.

Further development has improved the frequency response of the sensor. To achieve this a new shape of sensor has been adopted, consisting of a 1 x 10 mm strip of stainless steel coupled to a slab of ceramic (Fig 14). A more detailed description of the instrument is given by Salkield et al (1981).

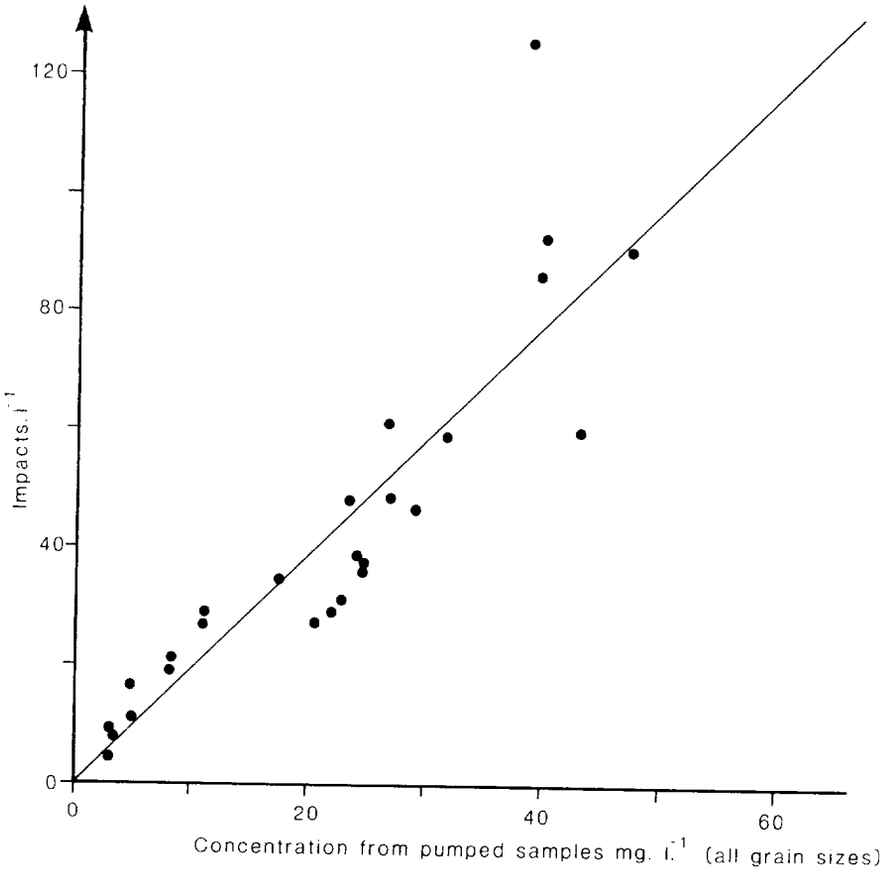

Fig 13: Field calibration of the disc-type sand transport probe.

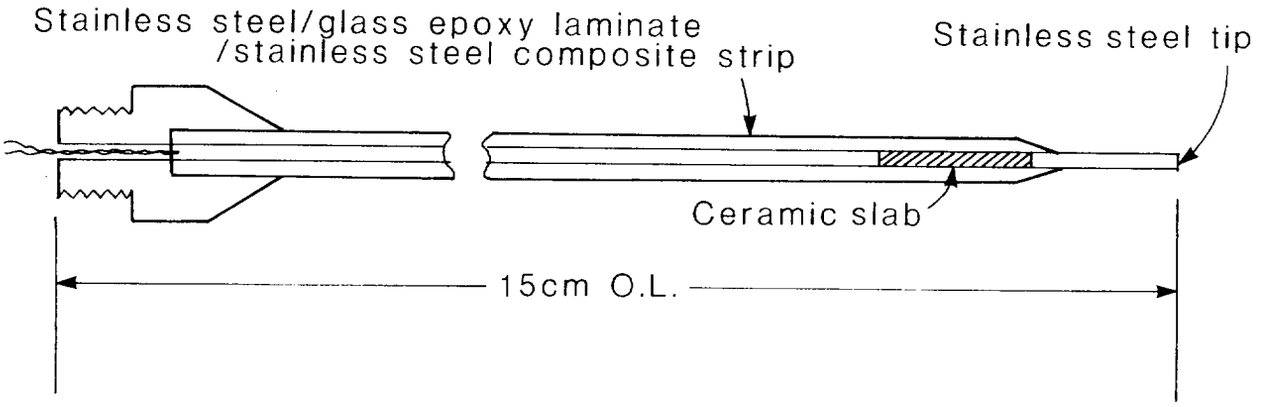

Fig 14: Construction of the strip-type sand transport probe.

2.9 Field experiment in the Taw Estuary

An experiment was performed in October 1980 in the estuary of the River Taw. The aims were (a) to test and calibrate the improved sand transport probe (STP), and (b) to obtain simultaneous turbulence data of suspended sediment concentration ($\overline{C}$ + c) and horizontal ($\overline{U}$ + u) and vertical ($\overline{W}$ + w) water velocities. A horizontal bar was erected at low water on drying sand flats, with the sand transport probe, an electromagnetic current meter (EMCM) measuring $\overline{U}$ + u and $\overline{W}$ + w, a pump sampling nozzle,and a Braystoke current meter mounted on it, their centre lines all being 18 cm above the bed. A second EMCM at a height of 56 cm measured the two horizontal components of velocity. A cable connected the instruments to a vehicle on the shore in which the signals were recorded.

The site comprised well-sorted rippled sand of median diameter 200 μm. The bed was formed into sandwaves (wavelength ≅ 20 m, height ≅ 80 cm), as is usual in an area with considerable sediment transport. The intruments were mounted near the crest of a sandwave, and daily levelling surveys made along a line passing through them (Fig 15) to establish the changing shape of the sandwaves. The flood tide is strongly dominant over the ebb here, producing a pronounced asymetry in the sandwaves, and causing them to migrate up-estuary at a rate of about 1.7 m per day over the spring tide period measured. The short term variations in bed level over one wavelength were monitored using self-recording stakes (Marks et al 1981). These showed ripples about 5 cm high migrating through one (unmeasurable) wavelength in about 30 min.

A number of practical problems were encountered, mainly because this was the first time we had performed this kind of experiment. The most important of these were:

(a) The pumping speed for the pumped samples was barely enough to keep the sediment suspended in the hose. This caused a long delay (up to 25 min) between the sediment entering the nozzle and arriving on the filter. Sediment also settled out in the hose. Thus the primary standard for calibrating the STP was of dubious quality.

(b) The threshold setting for the detection of impacts by the STP could probably have been set lower, decreasing the minimum grain size and hence increasing the impact rate observable.

(c) The axis of the instruments was some 20° out of alignment with the peak flood current. This caused sporadic 'stalling' of the EMCM head.

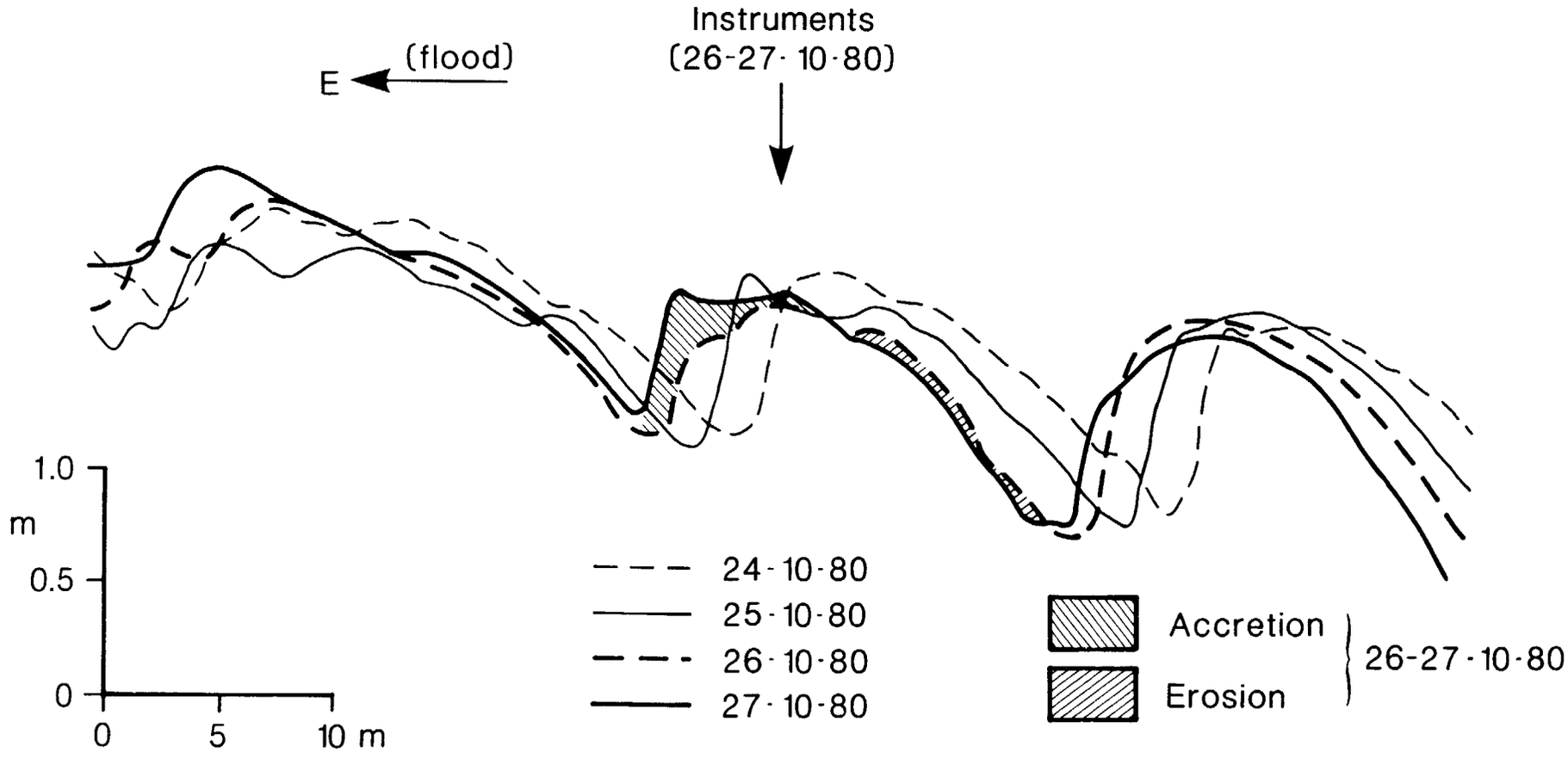

Fig 15: Daily levelling surveys of the bed topography around the instruments in the Taw experiment. The measurements described here were made during the flood tide which followed the deployment of the instruments at midday on 26 October 1980. Shaded areas denote the erosion and accretion which took place between 26 and 27 October on the instrumented sandwaves.

(d) The horizontal member carrying the instrument was not sufficiently rigid. Flow-induced vibration was found to produce a large spurious component in the vertical velocity signal of the EMCM, limiting its validity.

Methods were found of circumventing most of these problems at the analysis stage, but at the expense of extra analysis time and of much reduced reliability of the results. The deficiences were remedied in a further experiment, designed to investigate further some of the points of interest revealed by the 1980 experiment, which was performed in July 1982. Analysis of the data from the 1982 experiment is at an early stage, so only results from the 1980 experiment are presented here.

As was discussed in section 2.4, the rate of migration of bedforms is often used as a measure of the bedload transport rate. The Taw experiment affords a comparison of the transport deduced from the migration of both ripples and sandwaves with that obtained from the other measurements.

The ripple migration rate, assuming a ripple wavelength of 7 times the height, corresponds to a transport of about 900 gm cm^{-1} during the flood tide. The bedload transport rate was predicted from the formula of Bagnold (1980) using the values of grain size, water depth, and bed shear stress measured through the flood tide. The bedload transport integrated over the flood tide was about 2300 gm cm^{-1}. The mass of sediment moved as sandwave migration by the two flood and two ebb tides between the bed surveys of 26 and 27 October (Fig 15) corresponds to a transport through the crest of about 6000 gm cm^{-1} for one flood tide (the reverse transport due to the ebbs being assumed negligible). The suspended load transport rate was calculated using the formula given by Soulsby (1978) (a simplified version of Einstein's (1950) formula), with the values of grain size, water depth, bed shear stress, roughness length, and pumped suspended sediment concentration measured through the flood tide. The suspended transport integrated over the flood tide was about 25000 gm cm^{-1}.

The most contentious part of the bed and suspended load predictions was the estimation of τ_o. It was obtained by assuming a plausible value for the roughness length (z_o = 0.16 cm), and a logarithmic profile below z = 18 cm. However, numerical model predictions of τ_o (Dawson et al, 1983) show this to be inadequate, and a more rigorous approach should be adopted to give the above

results greater credibility. However, with this proviso we conclude that the ripple migration, while giving a lower bound to the bedload transport, underestimates it by about a factor 2. The sandwave migration exceeds the bedload transport. It gives a lower bound to the total transport, but in this case accounts for only 22% of it.

After allowing for the deficiences of the pumped sediment samples, a reasonable correlation was obtained with the STP, though not as good as that shown in Fig 13. The impact rate rose to about 1600 impacts per min at peak concentrations, proving the virtue of the slab ceramic design (Fig 14) for high-frequency measurements. (In the 1982 experiment impact rates in excess of 40,000 per min were recorded.) Three levels of pulse height were counted over 1 min periods, and these appeared to have a satisfactory relation with the observed grain size distribution. An analogue signal proportional to impact rate (at the lowest of the three levels) was recorded. It was converted to instantaneous concentration by dividing by the instantaneous horizontal velocity registered by the adjacent EMCM, and using the calibration against the pumped samples.

Examples of the turbulent concentration field measured by the STP are shown in Fig 16. As sediment begins to go into suspension (Fig 16a) individual grain impacts are seen, giving way to discrete clouds of sediment separated by clear water as the current speed increases. At the peak of current and concentration (Fig 16b) moments of clear water appear only infrequently, and the sediment concentration is almost continuous, though still highly variable. As the current speed and concentration die anyway (Fig 16c) the concentration becomes intermittent again, with clouds of sediment at concentrations many times the mean being advected past in 2 to 10 s.

The mean concentration $\overline{C}$ (Fig 17) rises rapidly once a mean current speed of about 50 cm s^{-1} has been exceeded. It reaches a peak in excess of 800 mg l^{-1} at about the same time as the peak of $\overline{U}$, and dies away again to small values when $\overline{U}$ falls below 50 cm s^{-1}. The rms current speed $(\overline{u^2})^{\frac{1}{2}}$ rises in line with $\overline{U}$ until 1710, when it falls and then remains steady until 1846, when it falls again in line with $\overline{U}$. The turbulent intensity $(\overline{u^2})^{\frac{1}{2}}/\overline{U}$ was thus lower during the period when sediment was suspended, the most marked effect being at the peak concentration. There are two possible reasons for this: the motion of the solid grains

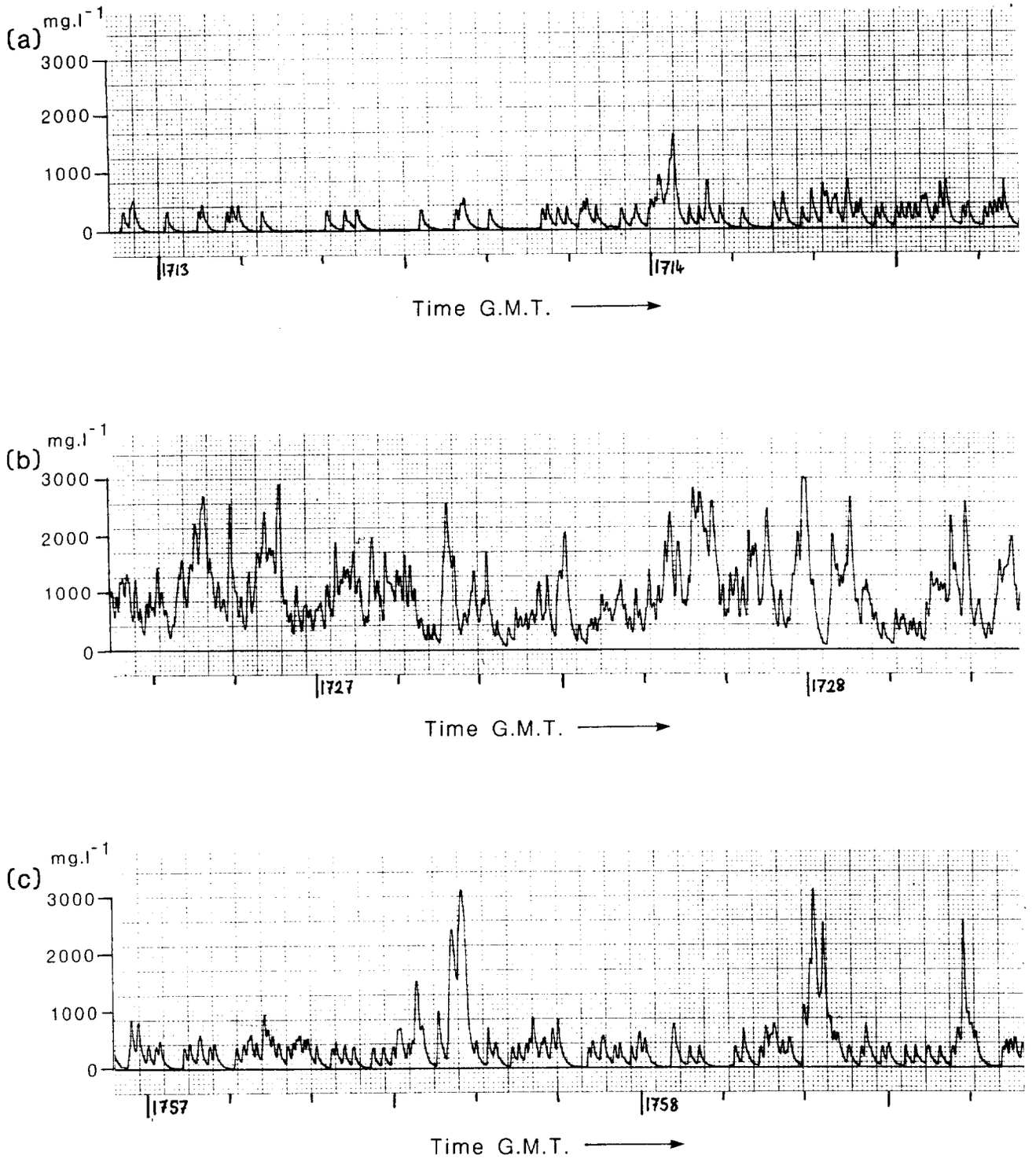

Fig 16: Analogue output from the strip-type sand transport probe in the Taw estuary. (a) Onset of detectable sediment transport (b) Highly turbulent concentration signal at the time of peak mean concentration (c) Decelerating flow with decreasing sediment concentration.

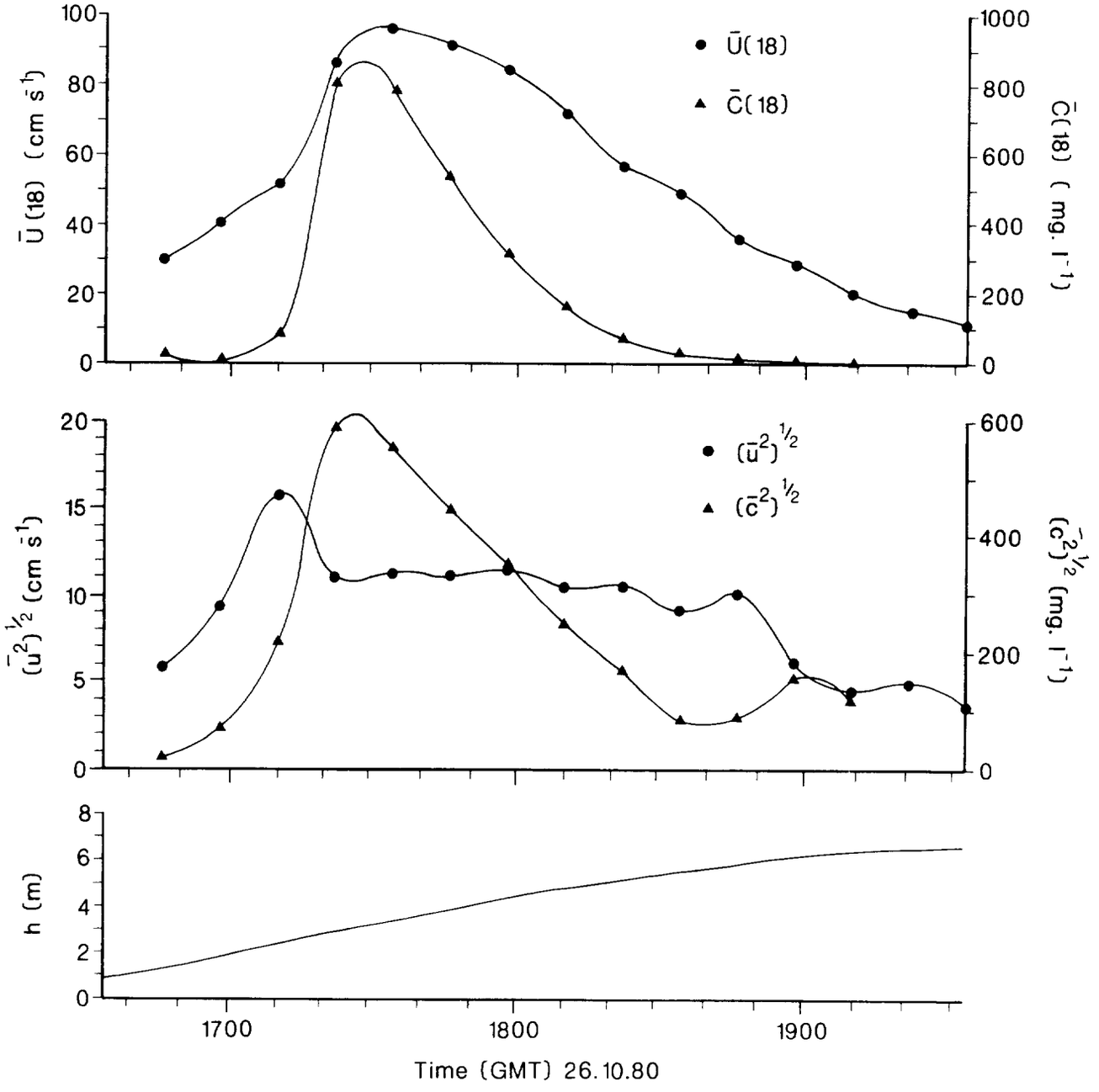

Fig 17: Mean and rms values of the velocity ($\overline{U}$ and $(\overline{u^2})^{\frac{1}{2}}$) and suspended sand concentration ($\overline{C}$ and $(\overline{c^2})^{\frac{1}{2}}$) measured 18 cm above the crest of a sandwave during a flood tide in the Taw estuary. The depth of water h at the site is also shown.

relative to the surrounding water will result in viscous dissipation of the turbulent kinetic energy in addition to that occurring in clear water; and the vertical density gradient produced by the suspended sediment will inhibit the production of turbulence because buoyancy forces must be overcome.

The first possibility has been tested by examining the Oseen-Boussinesq equation for grain motion. The ratio of energy dissipation by the grains to the dissipation in the water alone was found to be independent of grain size, but proportional to concentration. The maximum concentration encountered in the Taw experiment gave a value of 0.3% for the above ratio, so clearly the grain dissipation is unimportant in this case.

To investigate the second reason, the density stratification parameter z/L was calculated from the measured values of concentration and Reynolds stress. The turbulent intensity $(\overline{u^2})^{\frac{1}{2}}/\overline{U}$ was found to decrease with z/L (Fig 18), and a similar behaviour was observed for the intensities of the vertical component $(\overline{w^2})^{\frac{1}{2}}/\overline{U}$ (though this is complicated by the vibration referred to previously), and the Reynolds stress $(-\overline{uw})/\overline{U}^2$. Thus density stratification by the sediment appears to be the chief cause of the observed turbulence damping. This is the kind of effect which was discussed theoretically in section 2.7.

The kinematic Reynolds stress $-\overline{uw}$ (Fig 19a) reaches peak values of 17.0 and 18.2 dyne cm^{-2}, with a local minimum of 9.5 dyne cm^{-2} at about the time of maximum $\overline{U}$ and $\overline{C}$. The minimum may be due to density stratification effects, though it might alternatively be simply attributable to the large natural variability of stress measurements. Because of the complex topography, we cannot assume either a constant stress layer or a logarithmic velocity profile, so u_* is difficult to deduce. A numerical model for shallow flow over topography (Dawson et al, 1983), which was run with the surveyed topography and matched to the measured velocities and Reynolds stress at 1734, gave a bed shear stress of τ_o = 23.6 dyne cm^{-2}, and hence u_* = 4.9 cm s^{-1}. This must be regarded as the best available estimate.

The horizontal turbulent flux of sediment $\overline{uc}$ is found to be positive, ie diffusion is occurring in the downstream direction. It is relatively unimportant, however, as the measured values never exceeded 1.6% of the mean horizontal flux $\overline{U}\ \overline{C}$. In addition, the correlation $\overline{uc}/(\overline{u^2}.\overline{c^2})^{\frac{1}{2}}$ never exceeded

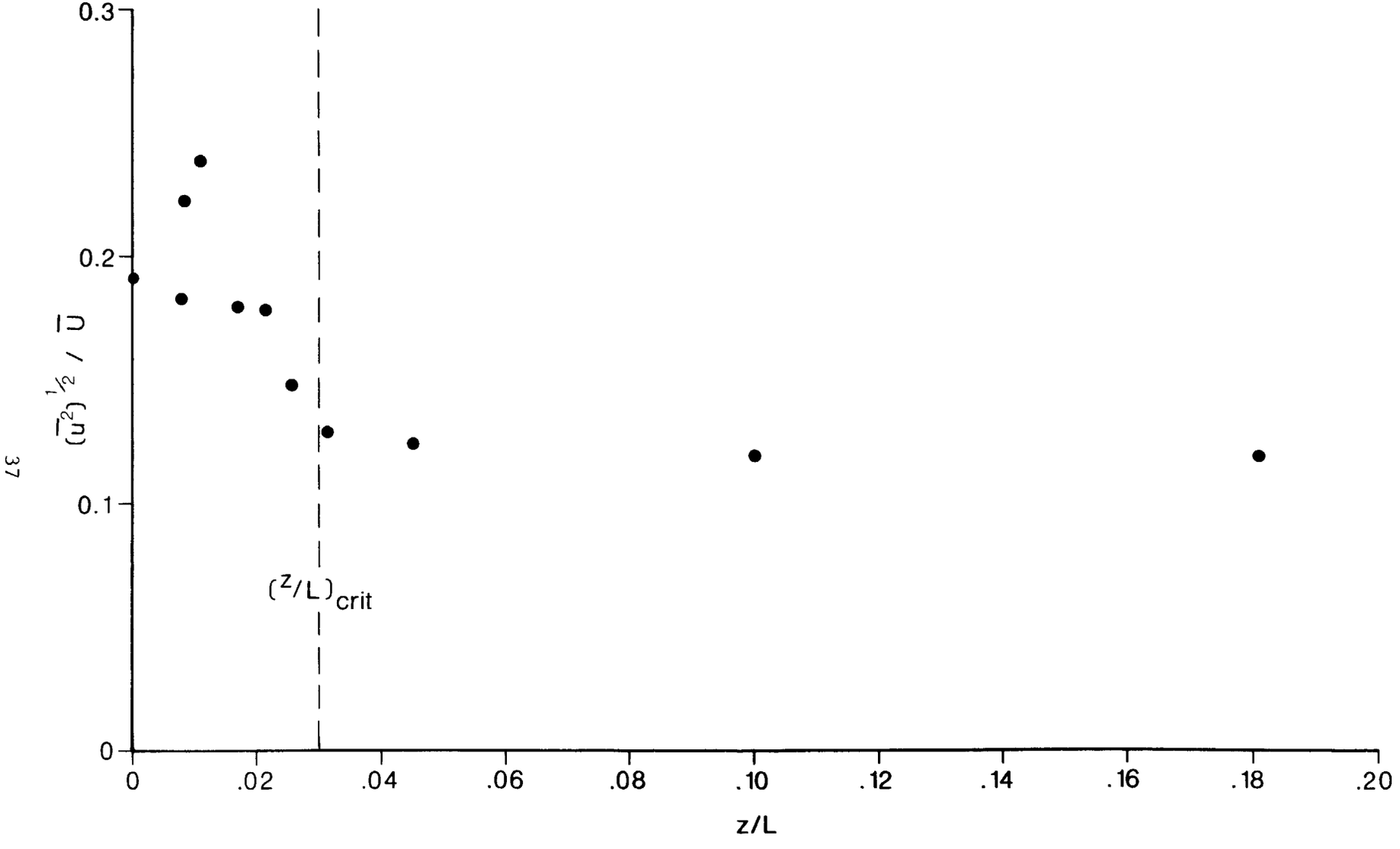

Fig 18: The variation of turbulent intensity $(\overline{u^2})^{\frac{1}{2}}/\overline{U}$ with the density stratification, parameterised by z/L, due to suspended sand. When z/L = 0.20, the equivalent gradient Richardson number is about 0.10.

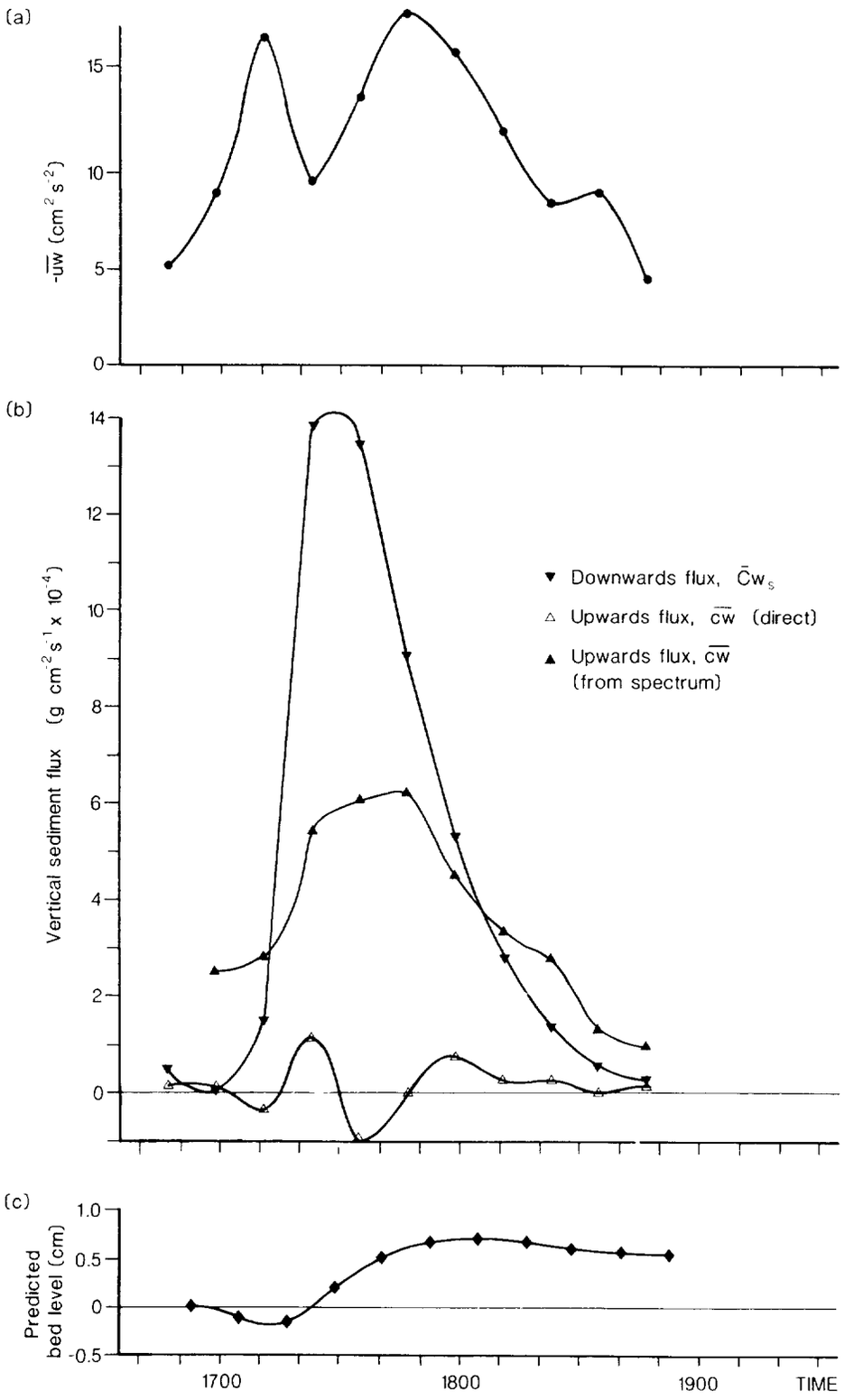

Fig 19: Vertical fluxes measured 18 cm above the crest of a sandwave during a flood tide in the Taw estuary. (a) The momentum flux, $-\overline{uw}$ (ie kinematic Reynolds stress). (b) The downward settling flux $\bar{C}w_s$, and the upwards diffusive flux $\overline{cw}$ of suspended sand calculated directly, and as deduced from the concentration spectrum. (c) The variation in bed level which would result from the difference between the upwards (indirect) and downwards fluxes.

0.11, indicating that although clouds of suspended sediment tend to occur at times of peak instantaneous horizontal velocity, the association is not a strong one.

The vertical flux $\overline{cw}$, on the contrary, is of great importance, as it is the mechanism by which sediment is put into suspension. If the concentration profile is not varying in space or time, the upward diffusive flux of sediment $\overline{cw}$ is equal to the downward flux due to settling, $\overline{C}w_s$, where w_s is the settling velocity of the sediment. The weighted mean settling velocity of the suspended sand obtained from the pumped samples is 1.71 cm s^{-1}, permitting the downward flux to be calculated (Fig 19). The upward flux can be calculated directly from the product of the fluctuating vertical velocity measured by the EMCM, and the fluctuating component of the concentration measured by the adjacent STP. The resulting values of $\overline{cw}$ (Fig 19) are found to be very much smaller than $\overline{C}w_s$, and even to be negative on two occasions. A negative value of $\overline{cw}$ would imply that the concentration is increasing upwards ($\partial\overline{C}/\partial z > 0$), causing a downwards diffusive flux, in addition to the settling flux. This is rather improbable at the site used. Furthermore, the correlation $\overline{cw}/(\overline{c^2}.\overline{w^2})^{\frac{1}{2}}$ took values within the range -0.04 to 0.04, ie practically zero.

We turn to the spectral and cospectral distributions for further information on the cause of the anomalous values of $\overline{cw}$. First we look at the energy spectrum of the concentration time series (Fig 20), from which the sizes of the clouds of suspended sediment can be deduced. The frequency has been converted to wavenumber k using Taylor's hypothesis, and the spectrum presented in equal area - equal energy form, as is usual for turbulence spectra. The wavelength $\lambda = 2\pi/k$ at the peak of the spectrum representing the length of the dominant clouds, is about 300 cm, and there are appreciable contributions from clouds with lengths a factor of 10 either side of this. Energy spectra of the horizontal and vertical velocities are also shown in Fig 20, though the latter has suffered considerable distortion due to the flow-induced vibration which appears around kz = 1.6. The peak of the concentration spectrum appears to fall between those of the horizontal and vertical velocities, though the true peak of the vertical velocity spectrum can only be conjectured.

The cross-spectrum of c and w is not seriously affected by the vibration problem, because only a correlated noise signal on the STP would have any effect.

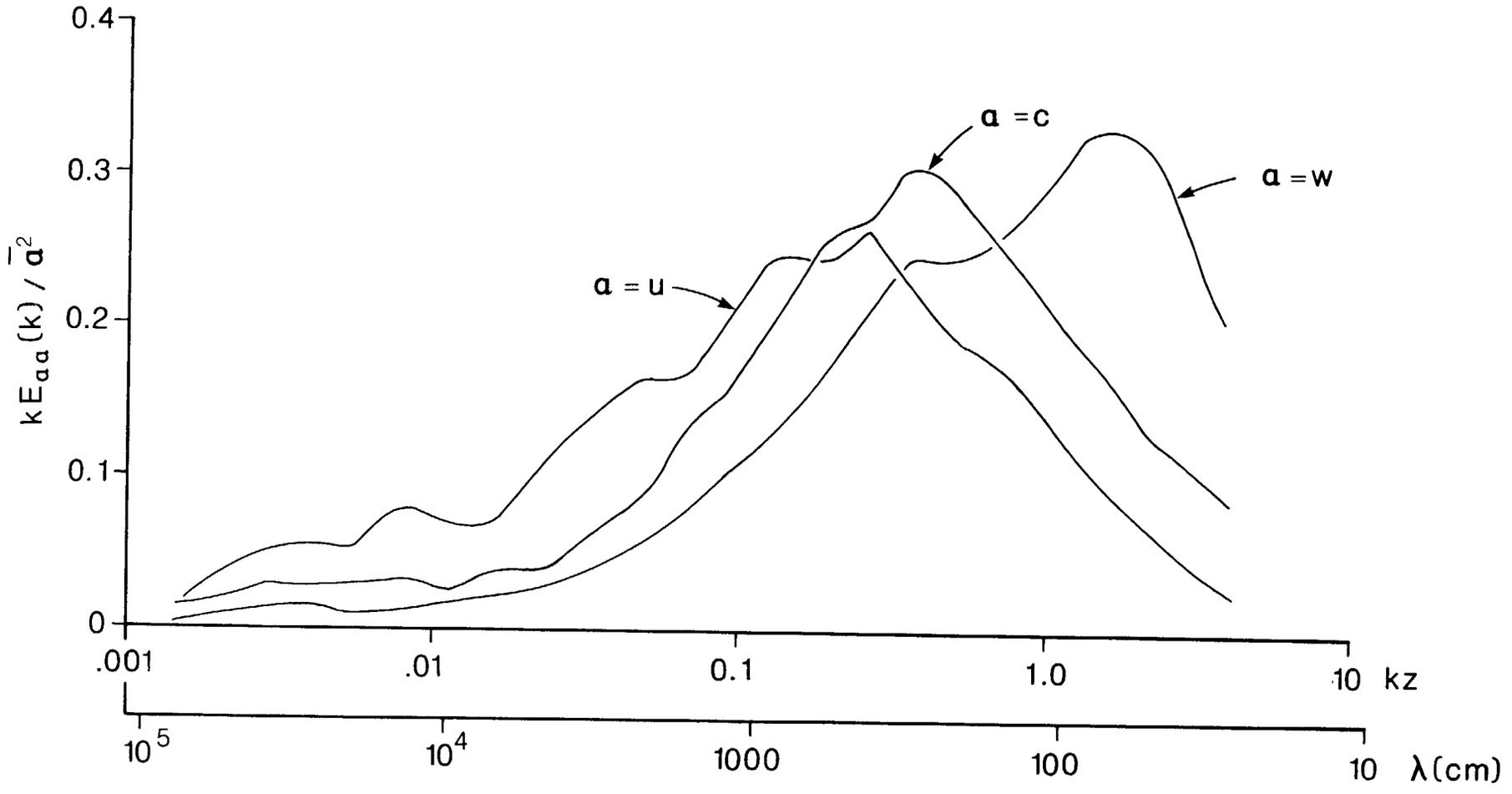

Fig 20: Energy spectra of u, w and c presented in normalised, wavenumber-weighted form. The abscissa in kz should have general significance, while that in λ is specific to the height and current speed of these measurements. The flow induced vibration affecting the w signal appears as a peak in the w spectrum, centred on kz = 1.6

Over the range of kz in which contributions from both c and w are appreciable ($0.09 < kz < 2.0$), the phase spectrum shows that c lags w by about 90°. This may be an artefact of the rate-meter circuit of the STP, though it is unlikely that it would affect such a wide range of frequencies. Otherwise the implication is that the peak value of the concentration follows a quarter-cycle behind the peak upwards vertical velocity. A possible explanation is that the grain velocity lags the water velocity because of the inertia of the grains. This was investigated by obtaining an appropriate solution of the Bassett-Oseen-Boussinesq equation of grain motion. The maximum lag which would be felt under the conditions of the Taw experiment would be only 2.4°, so this explanation can be discounted. An alternative explanation is that a cloud of sediment is drawn up from the bed following (not during) a burst, and a patch of clear water is drawn downwards following a sweep. The subject will be studied further using the 1982 Taw data, which has the benefit of new circuitry in the STP which will not introduce an artificial lag.

A plot of the spectra on log-log axes (not shown) reveals that the concentration spectrum closely follows a $k^{-5/3}$ law for wavenumbers $kz > 1$, indicating that the suspended sediment behaves as a turbulent scalar property of the flow. The u-spectrum, as usual, also follows a $k^{-5/3}$ law at large kz. This suggests an alternative approach to obtain values of the upward sediment flux $\overline{cw}$.

Direct measurement of the Reynolds flux of heat in the atmosphere can also be unreliable. An indirect method is sometimes used by micrometeorologists to derive better estimates of the heat flux, obtained from the $k^{-5/3}$ part of the temperature spectrum (Hicks and Dyer, 1972). We have adapted this method to obtain more reliable estimates of the vertical sediment flux, using the $k^{-5/3}$ part of the concentration spectrum. The tidal variation of $\overline{cw}$ calculated by the spectral method is shown in Fig 19; the results look more plausible than those obtained from the direct method. The upward flux exceeds the settling flux $\overline{C}w_s$ at the start of the tide, as sediment goes into suspension. Through the middle part of the tide the settling exceeds the upward diffusion, causing a net transfer of sediment towards the bed. As the current decelerates to slack water there appears again to be an excess of upward diffusion over settling. This is contrary to the expectation of a net settling out from suspension as slack water approaches, and, if valid, can only be true locally, with the eroded

sediment being advected downstream to settle elsewhere.

If the net flux of sediment upwards or downwards at the measuring height of 18 cm is interpreted as erosion or deposition of the bed beneath the instruments, the resulting variation in bed level through the tide is as shown in Fig 19c. The overall predicted accretion of 0.5 cm during the flood tide compares with a measured accretion of 2 cm over the 2 floods and 2 ebbs between successive levelling surveys. Sediment transport during the ebb tides is probably small, so we can assume a measured accretion of about 1 cm per flood tide. The agreement with the figure calculated from the fluxes is of the right order of magnitude, though the levelling figure is only accurate to about ±2 cm, and in the predicted figure no account has been taken of either the variation with height of the fluxes between the bed and the instruments, or the effects of bedload transport.

Having studied the Reynolds stress $-\rho\overline{uw}$ in terms of the bursting phenomenon (section 2.5), it is pertinent to investigate whether the measured sediment flux $\overline{cw}$ behaves similarly. In particular, we wish to enquire whether bursts of cw occur simultaneously with bursts of uw, and if so, what vertical flux of sediment accompanies a particular size of uw burst.

Because the w signal was noisy, the uw and cw time series are contaminated, so that a full analysis of their bursting characteristics is not justified. However, a visual examination has been made. An example of the simultaneous time series of w, c, cw and uw is shown in Fig 21. Peak values of c do sometimes occur at the same time as peak positive or negative values of uw, but there are many instances where a peak c does not correspond to a peak uw, and vice versa. Much the same is true for the correspondence between the cw and uw time series; however, the w signal is common to cw and uw, which biasses the signals in favour of some correspondence. No correlation between c and w is evident, as might be expected from the small values of $\overline{cw}/(\overline{c^2}.\overline{w^2})^{\frac{1}{2}}$ which were found.

A more quantitative comparison was made between the uw and c signals, to investigate whether large uw events were accompanied by high or low values of sediment concentration. Large events were chosen to be defined as those for which $|uw|$ exceeded 200 dyne cm^{-2}, this definition being simpler to apply visually than the definition used in section 2.5. Each selected event was classified in terms of u and w as a burst, sweep, up-acc or d-dec, according to the scheme

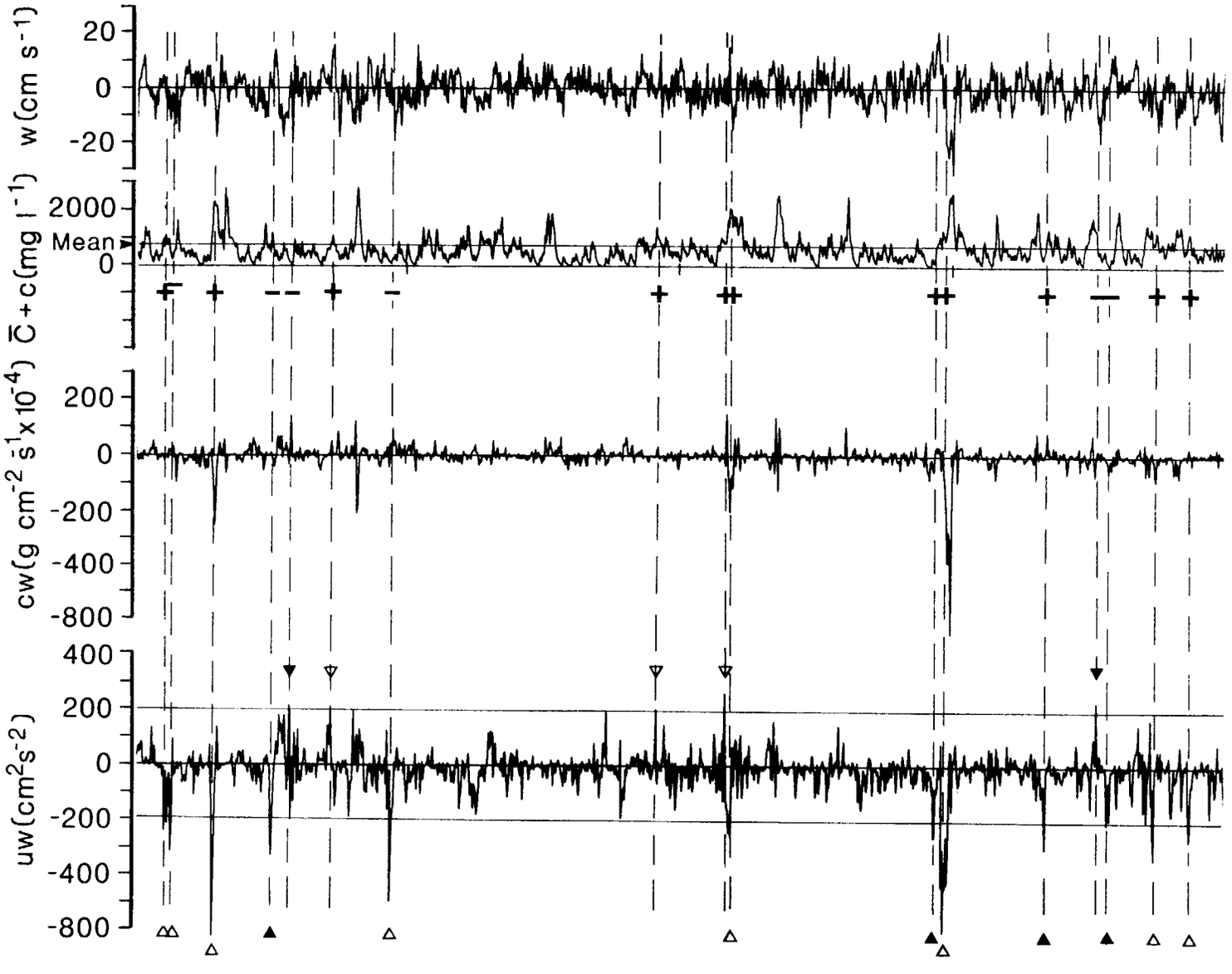

Fig 21: Three minute time series of vertical velocity, suspended sand concentration, instantaneous sediment flux and instantaneous momentum flux. Instants when $|uw| > 200$ cm^{2}s^{-2} are identified using the symbols defined in Fig 9. The value of the suspended sand concentration at the same instant are indicated as being either greater than (+), or less than (-), the mean concentration for the 12 min record from which this portion was taken.

shown in Fig 9. The corresponding value of c was noted as being either greater than (+) or less than (-) the 12 minute mean (Fig 21). This analysis was performed on a 48 min period around peak current, from 1716 to 1804 (Table 2).

Table 2: Number of occurrences of bursting events for which the suspended sediment concentration is greater than (+) or less than (-) the mean.

Concentration	Burst	Sweep	Up-acc	D-dec	Total
+	34	46	17	7	104
-	34	30	10	10	84
Total	68	76	27	17	188

As found in section 2.5, bursts and sweeps occur more commonly than up-accs or d-decs (despite the different definition of an event). The total number of pluses is rather greater than the total number of minuses, showing that overall an above-average concentration tends to occur during an event. Both sweeps and up-accs (the 2 kinds of event with $u > 0$) have appreciably more occurrences of high than of low concentration. Bursts, which might intuitively be expected to carry sediment up from the bed, in fact show equal numbers of occurrences of high and low concentration. Relatively few d-decs occurred, with these showing a weak preference for low concentrations.

The only comparable study of which we are aware was made by Gillette and Porch (1978), who obtained 'several minutes' of measurements of turbulent velocity and concentration data of dust settling in the atmosphere, downwind of an eroding dirt road. They too found that the greatest contribution to the transport was due to sweeps carrying dust-laden air. They attributed this to the fact that the dust was settling rather than eroding. However, in our case we would expect active diffusion of sediment up from the bed to be taking place.

The simple visual technique we have used takes no account of the phase difference between c and w seen in the cross-spectrum. Once again, it is hoped

that the July 1982 measurements will provide a more comprehensive data set for further study of the inter-relation between bursts of momentum and sediment suspension.

3. SEDIMENT TRANSPORT BY WAVES

3.1 Background

Since 1975 an attempt has been made at IOS Taunton to measure and interpret some of the basic features of sediment transport by waves in the sea (see Davies and Wilkinson (1977, 1979) and Davies (1980)). Almost all previous studies of this subject have involved either theoretical or laboratory work; comparatively little work has been carried out in the field. The theory has been concerned mainly with properties associated with surface waves, such as the wave induced motions in the body of the fluid and the nature of the oscillatory boundary layer above the bed, while the laboratory work has concentrated on the transition from laminar to turbulent flow in the wave boundary layer, with the threshold of sediment motion in oscillatory flow, and with aspects of ripple formation on the bed (see the review of Davies (1983)). The present study has been concerned, to a greater or lesser extent, with all of these matters. Very little previous work has been carried out on the sediment transport rates which occur when waves are present, due largely to the inadequacy of existing instrumentation. Although for a symmetrical to- and fro- wave induced motion the net sediment transport must be zero, the importance of wave action in the problem as a whole is its ability to mobilize sediment by generating large shear stresses within the thin wave boundary layer. If, for any reason, a steady current is superimposed on the wave action, the resulting net sediment transport rate may be unexpectedly large. Even small steady currents, not capable of causing sediment motion on their own, may be found to transport quite a substantial sediment load. However, before such effects can be treated at all adequately, it is necessary to achieve a basic understanding of the properties of sediment movement in comparatively simple situations in which the flow is oscillatory.

The principal differences between the idealized cases usually treated both in theory and in the laboratory, and the situation in the field, are, firstly, that sea waves are rather irregular and not simply sinusoidal and, secondly, that the seabed comprises a mixture of grain sizes and not a single size. Furthermore, mobile seabeds are generally rippled and not flat, and this further complicates

matters. The processes at work near the seabed depend rather critically upon whether or not ripples are present. If the bed is rippled, the near bed oscillatory motion may induce a pattern of vortex formation and shedding in each wave half cycle. This both stabilizes the rippled bed structure, and also picks the sediment up into the flow as a suspended load. More generally, vortex formation and shedding is associated with high wave drag coefficents and, hence, high wave energy dissipation rates. It is therefore a phenomenon of considerable practical importance. If the bed is flat, sediment entrainment by an oscillatory flow must result primarily from turbulent diffusion. At low flow stages, at or about the threshold of motion, wave drag coefficients tend to be an order of magnitude less than those for rippled beds. At high flow stages, when the ripples have been "washed out" by the oscillatory flow and there is a substantial sediment load, wave drag coefficients are also rather less than those for rippled beds (Grant and Madsen (1982)) and, consequently, wave energy dissipation rates are rather less than might have been expected.

The detailed aims of the present field study have been

(i) to determine the conditions at the threshold of sand motion in terms of the measured free stream velocity and to make comparisons with laboratory results;

(ii) to determine on a wave-by-wave basis whether the boundary layer was laminar or turbulent and also, for rippled beds, whether vortex formation and shedding was occuring;

(iii) to calculate bottom stresses at the threshold of motion on a wave-by-wave basis, and to compare, where possible, the skin friction component of the total stress with the Shields' threshold stress from the laboratory;

(iv) to determine a criterion for the onset of vortex formation above rippled beds, in terms of the ratio of observed ripple wavelengths and (deduced) orbital excursions of the near bed motion; and

(v) to determine the relationship between the observed equilibrium wavelengths of evolving sand ripples and the orbital excursions of those measured waves which were capable of moving sediment.

Under each of the above headings, a comparison has been made between the present field observations made in irregular waves, and previous laboratory results made

in idealized conditions. A final aim of the study has been to obtain a quantitative understanding of some of the features of separating flow over rippled beds from an irrotational flow model.

3.2 Field experiments

Four field experiments have been carried out at Blackpool Sands in Start Bay, S Devon, the two most recent of which, carried out in 1978 and 1980, have provided the basis for analysis on the present DoE contract. A description of the field site and information about the experimental method have been given by Davies and Wilkinson (1977, 1979). The aim of the experiments has been to measure the wave induced flow near the bed, and to monitor any associated sediment movement in order to determine the conditions at the threshold of motion. The flow observations have involved EMCM measurements at either two or three heights (between about 10 cm and 160 cm) above the bed, together with an associated measurement of the bottom pressure. The sediment motion observations have been made primarily with an underwater television system. Thus the analysis has been restricted to the determination of sediment threshold motion conditions, and has not provided any information about sediment transport rates. Unfortunately, attempts to quantify sediment motion with a "self-generated noise" (SGN) probe met with little success for the sand grain sizes at the field site. The experimental set up is shown in schematic outline in Fig 22a, and a representative 5 minute portion of the measured data is shown in Fig 22b. The rig was aligned by divers such that the dominant wave action was measured on the U-channels, as may be seen from the top two curves in the figure. (In fact, the variance of the V-component of velocity was greater in this run than in any other run.) Also included are the measured velocities obtained with the lower flowmeter, which show the vertical velocity to be negligibly small compared with the horizontal, as expected for relatively long waves. Associated with the velocity data in Fig 22b was a strong spectral peak centred on frequency 0.163 Hz (wave period 6.1 sec), suggesting a dominant surface wavelength of about 40-45 m in water of depth about 6 m. More generally through the experiments, swell waves were measured having periods in the range 10-13 seconds. The bottom pressure associated with the velocity records is shown in Fig 22b and, since this pressure may be seen to be very nearly in phase with the horizontal velocity, it follows that the waves at the field site were progressive waves which passed over the rig, and then dissipated their energy at the beach face with little energy being back reflected. Finally, observations of sediment motion are shown in Fig 22b in two forms; firstly, observations made on the basis of the synchronous underwater television records and, secondly, measurements made with

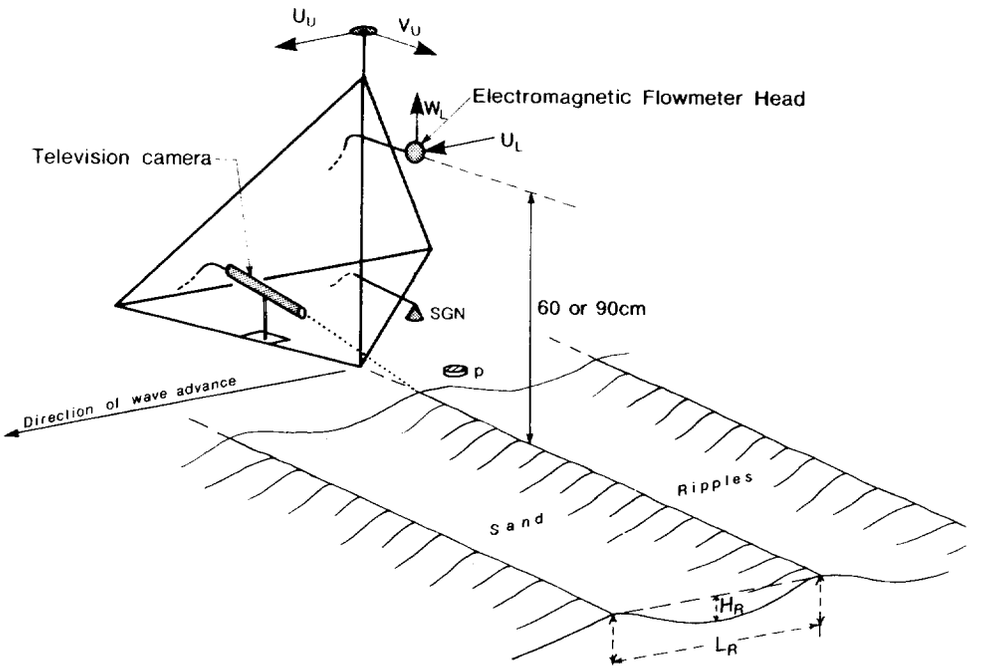

Fig 22a: Definition sketch. The range of water depths at the site of the rig was 4 - 9 m. Representative grain sizes (cm):

	d_{10}	d_{50}	d_{90}
1978	0.038	0.078	0.135
1980	0.015	0.026	0.062

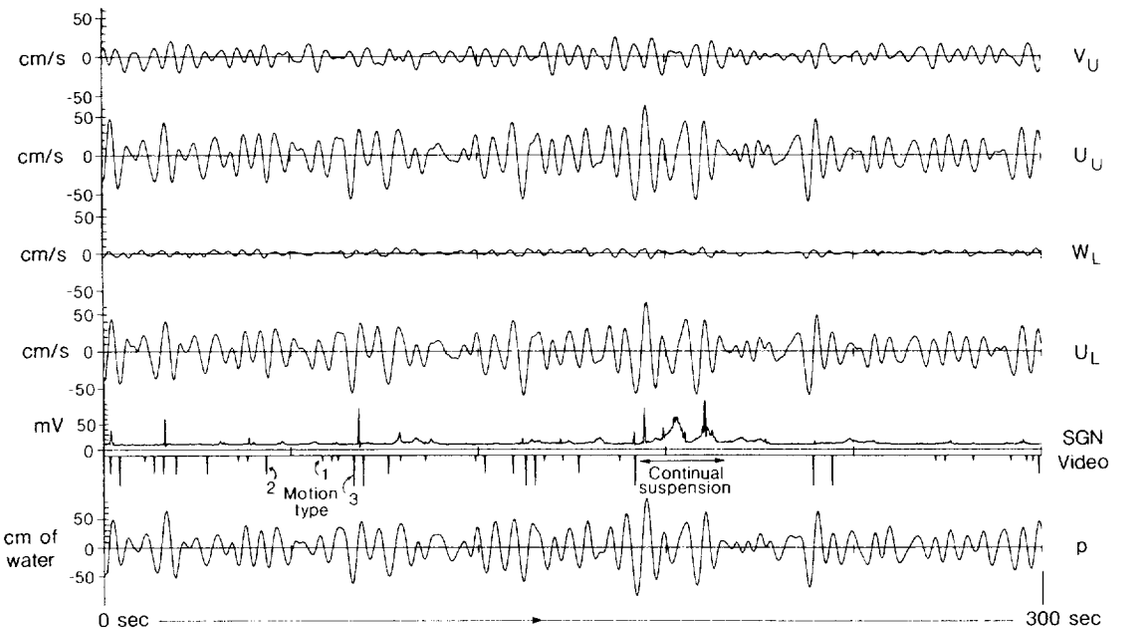

Fig 22b: Five minute portion of Run 10, 1980, for which the velocity measurements were made at heights of 160 and 60 cm (subscripts U and L, respectively) in water of depth about 6 m. Sediment motion results appear in the fifth row down: (i) filtered analogue SGN output above the zero line; (ii) observations from video records below the line, where motions are classified 1, 2 or 3, as defined in the text.

the SGN probe.

The wave boundary layer near the seabed is only centimetres thick if turbulent, and only millimetres thick if laminar. It is uncertain which flow regime exists in everyday conditions, though the flow is surely turbulent during storm activity. It is difficult to make observations this close to the bed in the field with conventional instrumentation. Attempts have been made to investigate this layer using time exposure photography of illuminated neutrally buoyant particles. The first of these, off the South Coast of England between Dartmouth and Mevagissey, failed due to the lack of a suitable field site. The second attempt took place in the Channel Islands, where the necessary conditions of clean sand (and thus reasonable visibility) with an appreciable amount of bottom water motion were found. The films obtained are at present being processed, and examples of the resulting photographs are shown in Fig 23.

3.3 Observations of sediment motion

The observations of sediment motion from the television records (shown in Fig 22b) involved the classification of each wave half cycle during the experiments as follows. The basic classification was between those wave half cycles in which sediment motion occurred and those in which it did not. A secondary classification of those half cycles in which sediment motion was observed was then made according to the numbering scheme 1, 2 and 3, where a wave was designated:-

1. if it caused the sporadic (incipient) to- or fro- motion of a few grains here and there on the bed;
2. if it caused a general to- and fro- bedload motion; or
3. if it caused the bed material to be taken into suspension.

Vertical bars of length comensurate with the above classification scheme are shown in Fig 22b for each of the waves which moved sediment; the absence of a bar indicates no motion. When the bed was rippled, the sediment motion was sometimes confined to the region of the ripple crests and, when it was flat (as it was at the start of the experimental run shown in Fig 22b), the motion occurred over the entire bed surface. It may be seen in Fig 22b that there is a reasonable correlation between the largest waves and the sediment motion observations of types 2 and 3, as expected.

The observations of sediment motion made on the rippled beds were of two

rather different kinds. In the 1978 experiment, the ripples were nonequilibrium features in the sense that they were not generated by the measured waves, but were left over from some previous wave activity. Above these ripples the flow was nonseparating for all the measured waves except the largest in the records, and sediment motion tended to be confined to the region of the ripple crests. In the 1980 experiment, the ripples evolved from an artificially flattened bed, and were thus in equilibrium with the measured waves. In this case, flow separation was a generally more common occurrence than was sediment movement; the motion itself tended to be over the entire bed surface, and the ripple wavelength was an order of magnitude smaller (5-20 cm) than in the 1978 experiment (50-80 cm).

The output of the SGN equipment which detected the self-generated noise of the moving sand particles, was compared with visual observations. As the particles move, they collide with each other and produce acoustic energy whose frequency is a function of their size, and amplitude is a function of the amount of sediment activity. This is picked up by a hydrophone and, after suitable electronic detecting, an analogue of the amplitude of the signal is produced as in Fig 22b. The wave half cycles were divided into categories 1 to 3 (as above, together with a '0', ie no motion, category) and examined for the presence of a signal from the SGN equipment. An example of the correspondence obtained is given in Table 2. Whilst this cannot be considered as good, it can be seen that the best agreement is realised if the threshold of the equipment is assumed to have been between the event types 2 and 3. The grain size present in these trials (median diameter d_{50} = 0.021 cm) was possibly at a lower limit of feasibility of this technique. This instrument, with different signal processing electronics has been tested recently in a tidal flow with gravel sized material, and has given good agreement with visually observed motion and threshold criteria from the literature. Further field testing and laboratory development is in progress.

Table 2: Example of Correspondence between SGN and visual observation of Sediment Motion

Threshold assumed to be between events of type	Agree	Disagree	Percentage Agreement
0 - 1	101	91	53
1 - 2	116	76	60
2 - 3	132	60	68
> 3	116	76	60

3.4 The threshold of sediment motion

A convenient method of presenting results of the type shown in Fig 22b is in the form of a histogram. An example for the 1978 data is shown in Fig 24 in which the peak horizontal velocity in a wave half cycle (measured at a height of 130 cm above the bed) is plotted on the horizontal axis, and the number of half cycles having peak velocities falling in each unit incremental range is plotted on the vertical axis. It may be seen that comparatively few waves had peak velocities in excess of 30 cm s^{-1}. More generally, the bimodal shape of the histogram is associated with the prevailing pattern of irregular swell waves. As far as sediment movement is concerned, it may be seen from the shaded regions in the histogram that, for velocity amplitudes less than about 10 cm s^{-1} in both directions, no sediment movement occurred; between about 10 and 30 cm s^{-1}, a proportion of the measured waves caused incipient sediment motion; above about 20 cm s^{-1}, a significant proportion of the measured waves caused general bedload motion; and, above about 30 cm s^{-1}, all the measured waves caused general motion. No wave velocities were sufficient to cause the coarse sand (d_{50} = 0.078 cm) to be suspended. On the basis of the figures quoted above, representative values for the threshold velocity amplitude for incipient motion and for general bed load motion may be taken as 20 and 25 cm s^{-1}, respectively. These estimates are based upon peak values of the U-component of horizontal velocity measured above the rig, and take no account of the (smaller) V-component. However, if a histogram is based upon peak values of the "total velocity" defined by $\sqrt{U^2 + V^2}\ \mathrm{sgn}(U)$, it is found that the equivalent estimates of the threshold velocity amplitude are, to all intents and purposes, the same.

The present experiments (Fig 24) were carried out on a rippled bed of representative steepness $\frac{H_R}{L_R}$ = 0.15 - 0.16 (symbols defined in Fig 22), and

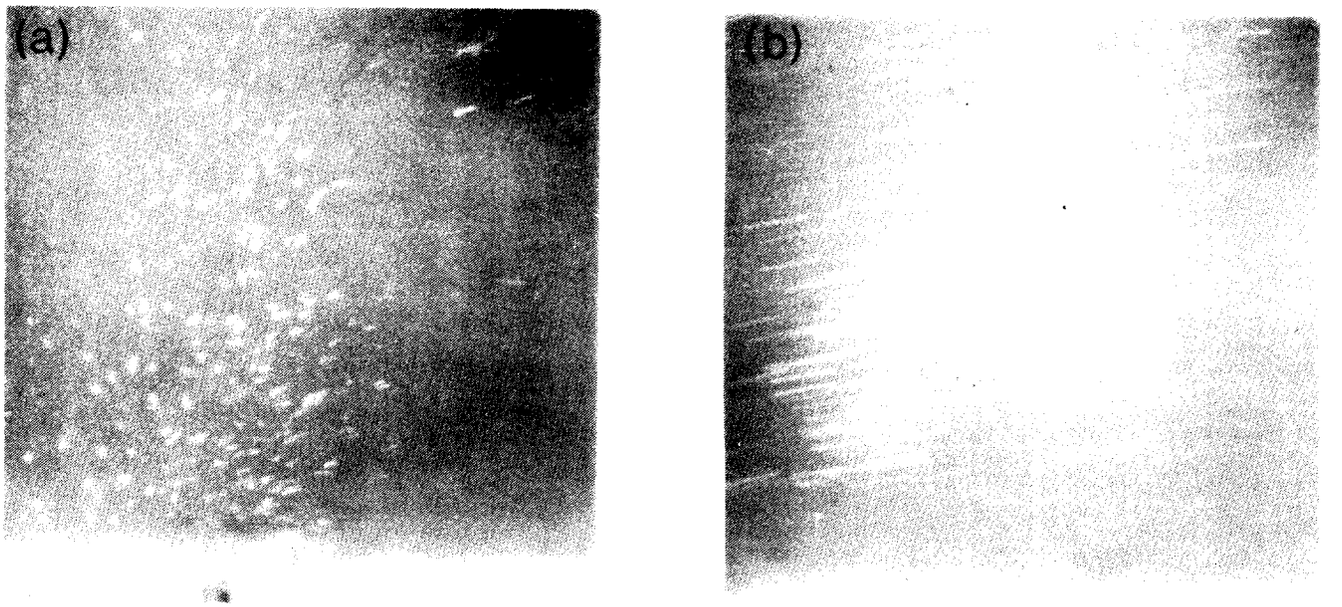

Fig 23: Examples of streaklines obtained by time exposure photography of neutrally buoyant particles under wave action: (a) at end of wave cycle and (b) in middle of wave cycle.

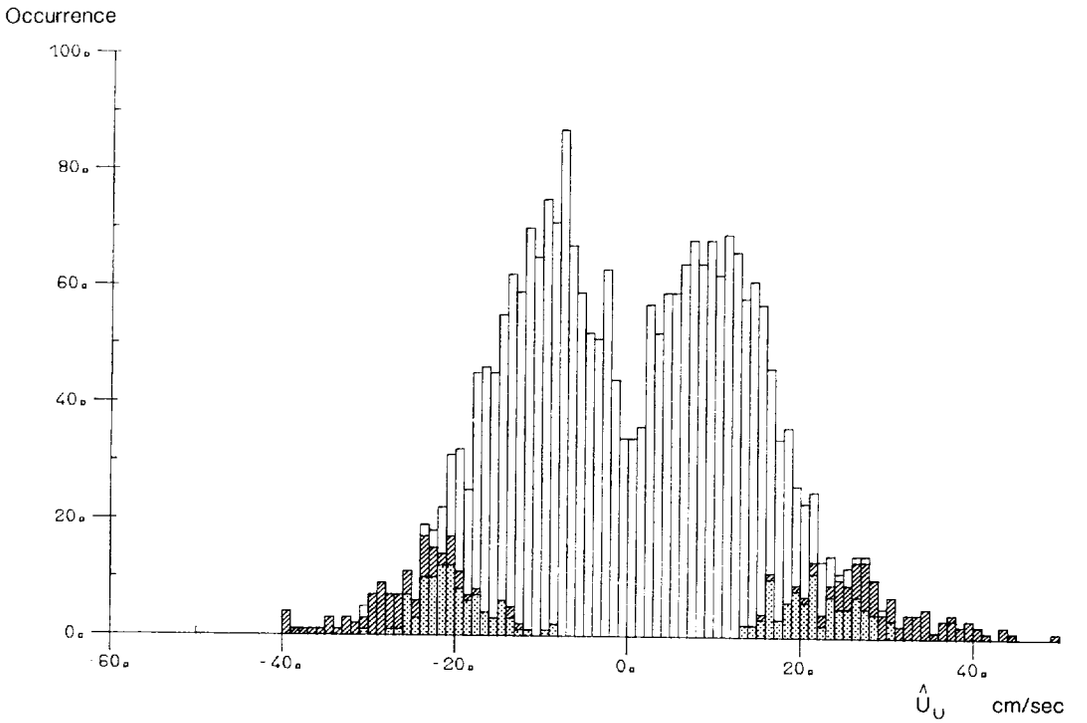

Fig 24: Histogram for Runs 8-14, 1978, showing the number of values of free stream velocity amplitude falling within each unit velocity range. The results are for a rippled bed on which sediment motion was of bedload type and occurred in the region of the crests only. Light shading (dots) denotes "incipient motion"; dark shading (hatching) denotes "general motion". Negative velocity amplitudes relate to motion in the seaward direction, and positive values relate to the shoreward direction. Representative values:

d_{50} = 0.078 cm, H_R = 12 cm, L_R = 77 cm

(Steepness $H_R/L_R \simeq 0.15$)

sediment motion was observed in the region of the ripple crests only. It follows that direct comparisons between the threshold values quoted above and previous threshold velocity values determined in the laboratory are not possible, since in the latter case the experiments were carried out with flat beds. It is possible, however, to correct the threshold velocities on the rippled beds, and thus enable comparisons to be made, by following the procedure suggested by Davies (1979, 1982). This procedure relates a measured velocity "well away" from the bed, say one ripple wavelength above it, to the velocity "close to" the rippled surface. However, the procedure is valid only if the flow is nonseparating, and if the boundary layer thickness is small compared with the ripple wavelength. As will be seen later, in section 3.5, the flow was fully separating for only a minority of the waves making up Fig 24, and so the flow pattern, in a frictionless sense, was generally similar to the idealized streamline pattern shown later for non-separating flow in Fig 31a. Also for the measured waves in the 1978 experiment, the boundary layer thickness has been found to be two orders of magnitude smaller than the ripple wavelength; this has been established by an argument equivalent to that used by Davies (1980). For the ripples in question, the representative near bed (potential) velocity in the region of the ripple crests has been calculated to be about 1.80 times the measured velocity. The respective threshold velocities for incipient and general bedload motion on a notional flat bed may therefore be taken as $1.80 \times 20 = 36$ cm s^{-1} and $1.80 \times 25 = 45$ cm s^{-1}. These values compare quite well with laboratory values for the threshold of motion on flat beds; the formulae of Bagnold (1946), Manohar (1955) and Komar and Miller (1975), suggest velocity amplitude values at the threshold of motion of sand having $d = 0.078$ cm ($=d_{50}$ of the bed material at Blackpool Sands) of 32, 40 and 33 cm s^{-1} respectively, and for sand having $d = 0.135$ cm ($= d_{90}$ at Blackpool Sands) of 41, 44 and 42 cm s^{-1} respectively. These calculated values are based on a representative wave period for the waves which moved sediment of 10 sec. Bagnold's formula is for the "first motion" (ie incipient motion) of grains on a flat bed, in what was stated by Bagnold to be a laminar boundary layer flow. Manohar's formula is for general bed load motion in a turbulent boundary layer flow. Komar and Miller's formula is based upon the results of five previous laboratory studies, including those of Bagnold and Manohar, and it therefore encompasses a wide range of conditions. Each of the laboratory formulae was obtained on the basis of experiments conducted with purely sinusoidal waves.

A more rational way of establishing sediment threshold motion conditions

under irregular waves in the field involves the calculation of the bed shear stress itself. The approach adopted here has been to calculate the peak bed shear stress $\hat{\tau}_0$ in each (assumed sinusoidal) wave half cycle from the equation $\hat{\tau}_0 = \frac{1}{2}\rho f_w \hat{U}^2 \mathrm{sgn}(\hat{U})$, where ρ is the fluid density, f_w is the wave drag coefficient of Jonsson (1966), and $\hat{U}$ is the peak value of the U-component of horizontal velocity. (Again, in practice, very minor variations in the results occur if the total velocity $\sqrt{U^2 + V^2}\,\mathrm{sgn}(U)$ is considered instead of U.) There are two ways in which this equation can be applied for rippled beds. On the one hand, $\hat{U}$ may be taken as the measured velocity "well away" from the bed, in which case the corresponding drag coefficient must be based upon a bed roughness defined in terms either of the ripple size, or both the ripple size and the grain diameter. The calculated value of $\hat{\tau}_0$ is then the <u>total</u> stress on the bed (the sum of skin friction and form drag), and the calculated drag coefficient itself is the appropriate one to use in estimating total wave energy dissipation rates. On the other hand, at least if the flow over the ripples is nonseparating, $\hat{U}$ may be taken as the near bed velocity just above the thin wave boundary layer, which may be calculated from the potential flow argument discussed earlier. The corresponding drag coefficient must then be based upon a bed roughness defined in terms of the grain size, and the resulting bed shear stress comprises the <u>skin friction</u> component of the total stress only. Since it is the skin friction which is "felt" by the grains, it is this part of the total stress which it is relevant to compare with threshold stresses determined in the laboratory on flat beds. The former procedure involving the calculation of the total stress has been adopted for the analysis of much of the 1980 data for which the flow was frequently separating, and the latter procedure involving the calculation of the skin friction has been adopted for the 1978 data for which the flow was generally nonseparating.

Some typical results for the portion of the 1978 data corresponding to that in Fig 24 are shown in histogram form in Fig 25. The equivalent bed roughness has been taken equal to the commonly recommended value of 2 x d_{90} (Kamphuis, 1975) where d_{90} is the size compared with which 90% of the grains are finer, and a value of f_w has then been calculated for each wave half cycle from Jonsson's (1966) criteria. The peak bottom stress in each (assumed sinusoidal) half cycle has been determined from the quadratic law quoted above, in which $\hat{U}$ has been based upon the (deduced) U-component of the near bed potential velocity in the region of the ripple crest. The histogram in Fig 25, which has peak stress in incre-

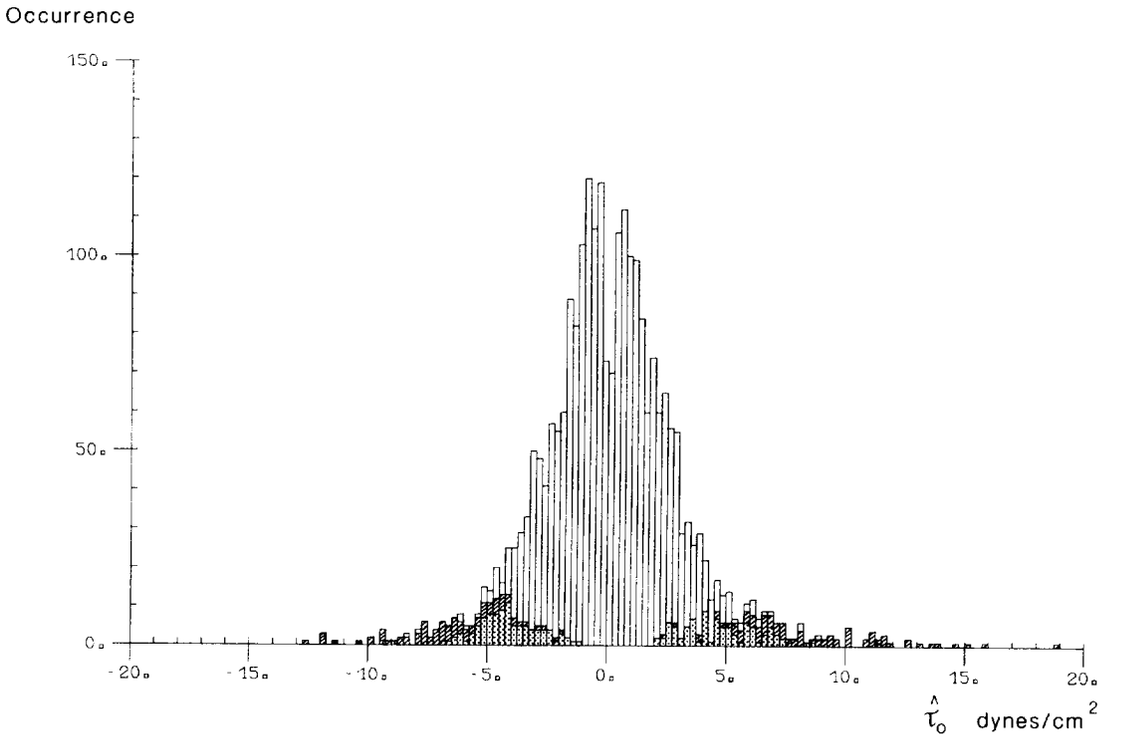

Fig 25: Histogram equivalent to that in Fig 24, but with the amplitude of the calculated bed shear stress (skin friction) plotted on the abscissa.

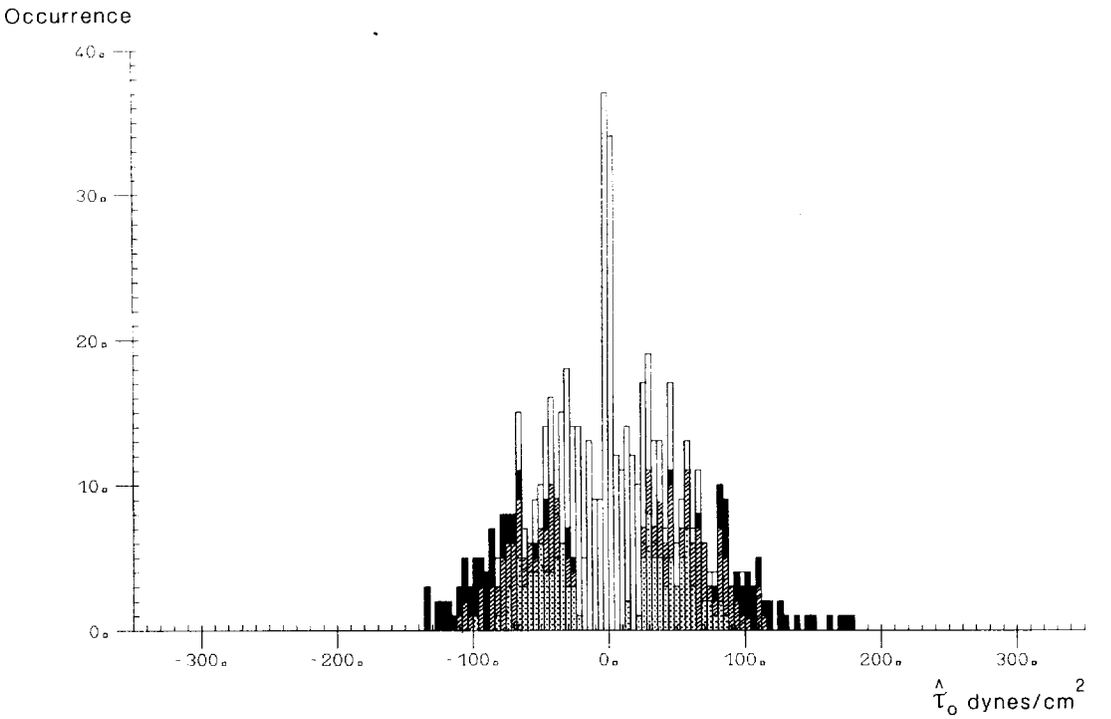

Fig 26: Histogram for Run 11, 1980, showing the amplitudes of the total shear stress on a rippled bed having $L_R \simeq 20$ cm, $H_R \simeq 2.9$ cm ($d_{50} = 0.026$ cm). Light shading denotes incipient motion; dark shading denotes general bedload motion; and black shading denotes sediment suspension. When motion was of any of the above types, it occurred over the entire bed surface.

mental ranges plotted on the abscissa, is not as clearly bimodal as that in Fig 24; this is due, in part, to the nonlinear nature of the stress calculation. The representative values of threshold stress for incipient and general bed load motion, analogous to the values obtained earlier for threshold velocity amplitude from Fig 24, are 3 and 6 dyne cm^{-2}, respectively. These values may be compared with laboratory determinations of the threshold stress of 4.1 and 7.6 dyne cm^{-2} for the grain sizes $d = d_{50} = 0.078$ cm and $d = d_{90} = 0.135$ cm, respectively. The histogram results are in fair agreement at least with the more important former value for the median grain diameter (d_{50}), and this confirms the validity of the present approach for the calculation of the bed shear stress in non-separating flow. Evidently, much uncertainty remains in the results in Fig 25 as far as threshold motion conditions are concerned. However, since this is due to sedimentological and other reasons, it is probably unrealistic to hope to eliminate it entirely by further refining the present arguments.

Calculations of the <u>total</u> stress have been made for the (often separating) flow conditions above the rippled beds in the 1980 experiment. The stress in such cases has been calculated on the basis of an equivalent bed roughness equal to $25\left(\frac{H_R}{L_R}\right) \cdot H_R$ (Nielsen, 1979), and values of f_w have again been calculated for each wave half cycle from Jonsson's (1966) criteria. The results obtained suggest that the total stress is an order of magnitude greater than the skin friction; this conclusion has been reached by comparing calculated total stresses in wave half cycles which just moved sediment, with known values of the threshold stress from Shields' curve. A typical histogram which illustrates this is shown in Fig 26, for a case in which there was both bedload and suspended load motion. The <u>total</u> stress at the threshold of bedload motion was about 30 dyne cm^{-2}, which may be compared with the much lower (skin friction) threshold stresses from Shields' curve of 2.0 dyne cm^{-2} ($d = d_{50} = 0.026$ cm) or 3.3 dyne cm^{-2} ($d = d_{90} = 0.062$ cm). This discrepancy suggests that form drag makes a dominant contribution to the total shear stress on a rippled bed in oscillatory flow and, in this respect, oscillatory flow differs from steady flow for which form drag and skin friction are generally considered to be about equal. The essential qualitative difference between the two cases is that, in oscillatory flow, the vortices formed above a rippled bed are shed into the flow in each wave half cycle whereas, in steady flow, the vortices remain trapped above the bed. An adequate understanding of the process of vortex formation and shedding above the bed is clearly necessary if the nature of the bed shear stress is to be fully understood.

3.5 Vortex formation above rippled beds in oscillatory flow

The video records which were used to determime conditions at the threshold of sediment motion have been used also to study vortex formation and shedding above the rippled beds in both the 1978 and 1980 experiments. In general, it was possible to see the near-bed flow quite clearly from the motion of particulate matter in the water. However, in some runs, dye crystals were placed on the bed to give a more distinct impression of the fluid motion. On this basis, each wave half cycle in the experiments was classified according to whether or not flow separation occurrred. When separation occurred, it was possible to observe a discrete vortex above the lee slope of the ripple, though it was not possible to estimate its size, or its associated internal velocities, with any accuracy. Often a vortex could be seen to be dragging sand towards the ripple crest, in the direction opposite to that of the outer free stream flow. Upon flow reversal, vortices could generally be seen to be carried away over the ripple crest, sometimes retaining their identity for sufficient time to be recognizable as discrete vortices on the other side of the crest. A typical portion of measured record illustrating waves which gave rise to some of these features is shown in Fig 27. Between the two extremes of separating and nonseparating (or contouring) flow, there was an intermediate class of wave half cycles in which the flow was clearly unstable above the lee slope of the ripple, but in which a discrete vortex did not appear to form. The term 'instability' is used here to classify wave half cycles in which perturbations of this kind were observed; it should be emphasized, however, that these perturbations in the flow were unlike those associated with turbulence in the usual sense. In Fig 28, histogram results are presented for the same portion of the 1978 data which gave rise to Fig 24, but in which the shaded regions now depict waves during which there was flow instability or vortex formation. Representative values of the measured U-component of horizontal velocity amplitude at the onset of instability and vortex formation are about 21 and 25 cm s^{-1}, respectively. Although these estimates are almost equal to those quoted earlier for the threshold of incipient and general bedload motion, this has no general significance.

Laboratory work on oscillatory flow above rippled beds has suggested that the flow starts to become unstable when the orbital excursion is approximately equal to the ripple wavelength (L_R), and that vortex formation occurs when the orbital excursion is rather greater than the ripple wavelength (Sleath, 1975). In order to test this criterion, an approximate orbital excursion ($2\hat{U}.\Delta T/_{\pi}$)has been

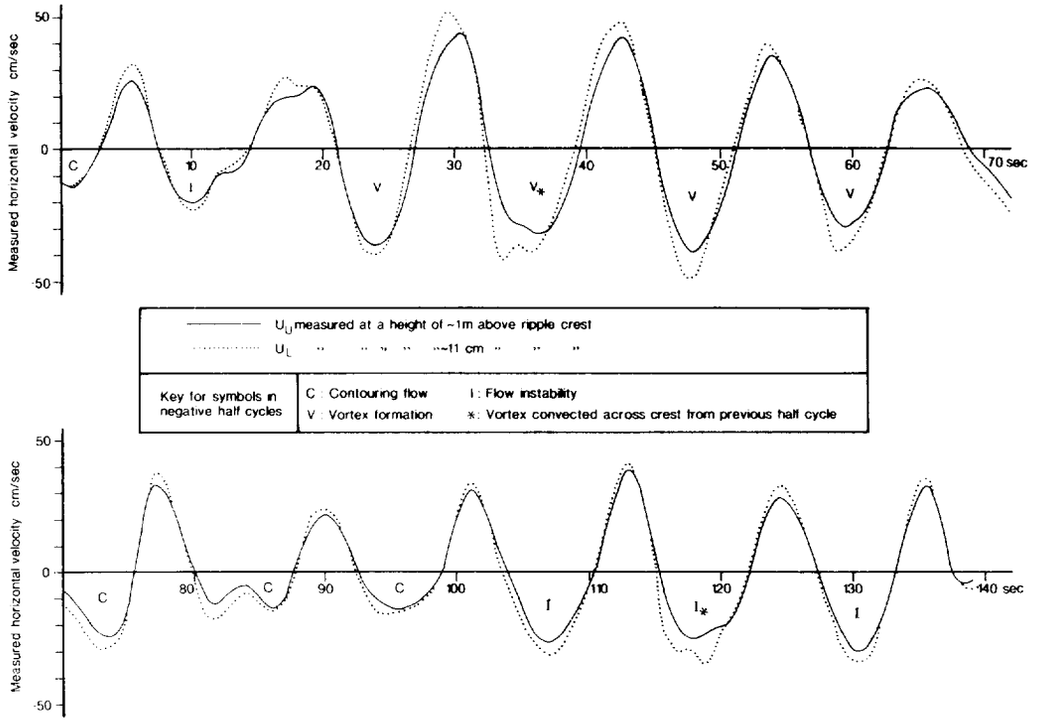

Fig 27: Portion of recorded horizontal velocity data (from Run 9, 1978) made above the crest of a ripple (L_R = 74 cm, H_R = 12 cm). In the two wave half cycles marked with an asterisk, the lower velocity record has a perturbation which was associated with the passage of a vortex below the EMCM measuring head.

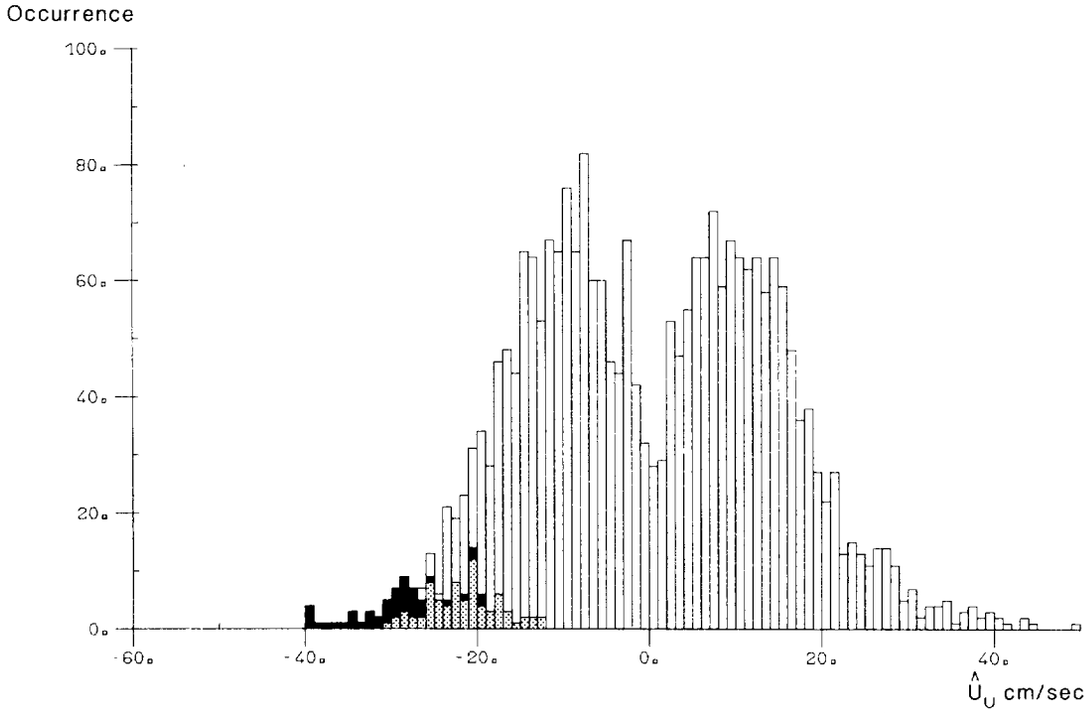

Fig 28: Histogram for the same data set as in Fig 24 (Runs 8 - 14, 1978). Light shading now denotes flow "instability"; black shading denotes vortex formation. Since the flow above only one side of the ripple was clearly visible on the underwater television records, results for instability and vortex formation are included only for those half cycles having negative peak velocities.

calculated for each of the wave half cycles contributing to Fig 28, based upon the assumption that each half cycle was sinusoidal, and characterized by its peak velocity ($\hat{U}$) and zero crossing half-period (ΔT). Half cycles which obviously violated this assumption by having two or more velocity maxima between zero crossings have been discarded. Thus, in Fig 29, a histogram based upon calculated orbital excursions associated with the measured U-component of horizontal velocity, but otherwise equivalent to that in Fig 28, has been obtained. Unlike Fig 28, the new histogram is not bimodal, due to the preponderance of low orbital excursion values. More importantly, the shaded region in the left tail of the histogram (the only tail for which results were obtained) suggests representative orbital excursion values of about 70 cm and 100 cm for the onset of flow instability and vortex formation respectively. These values may be compared with the ripple wavelength of 77 cm, and thus support quite well the earlier laboratory criterion for the onset of instability. This procedure has been repeated for all the relevant runs, and it has been found consistently that instability is associated with those waves having calculated orbital excursions greater than the ripple wavelength.

In the 1980 experiment, certain runs were carried out with an initially flat sand bed, which deformed into an (equilibrium) rippled bed during the recording period. The first signs of ripple formation tended to occur almost immediately after the flattening of the bed. Typically, a short period during which the ripples were of "rolling grain" type (Sleath, 1976) was followed by a longer period of ripple consolidation and growth during which the ripples were of "vortex type" (see Nielsen, 1979). The length of the entire process of ripple growth was of the order of 1 hour when only a few occasional waves exceeded the threshold of sediment motion, and it was rather more rapid with more active waves. In Fig 30 a typical histogram of calculated orbital excursions is shown for one of the 1980 ripple growth experiments. The representative orbital excursion for the waves which moved sediment may be seen from the shaded regions to have been in excess of about 30 cm, which may be compared with the rather smaller observed ripple wavelength for the run of about 10 cm. Similar results have been obtained in the other trials carried out. This confirms that ripple wavelengths caused by irregular waves in the field are of the order of, though rather less than, the orbital excursions of those waves which move sediment, as expected from laboratory work.

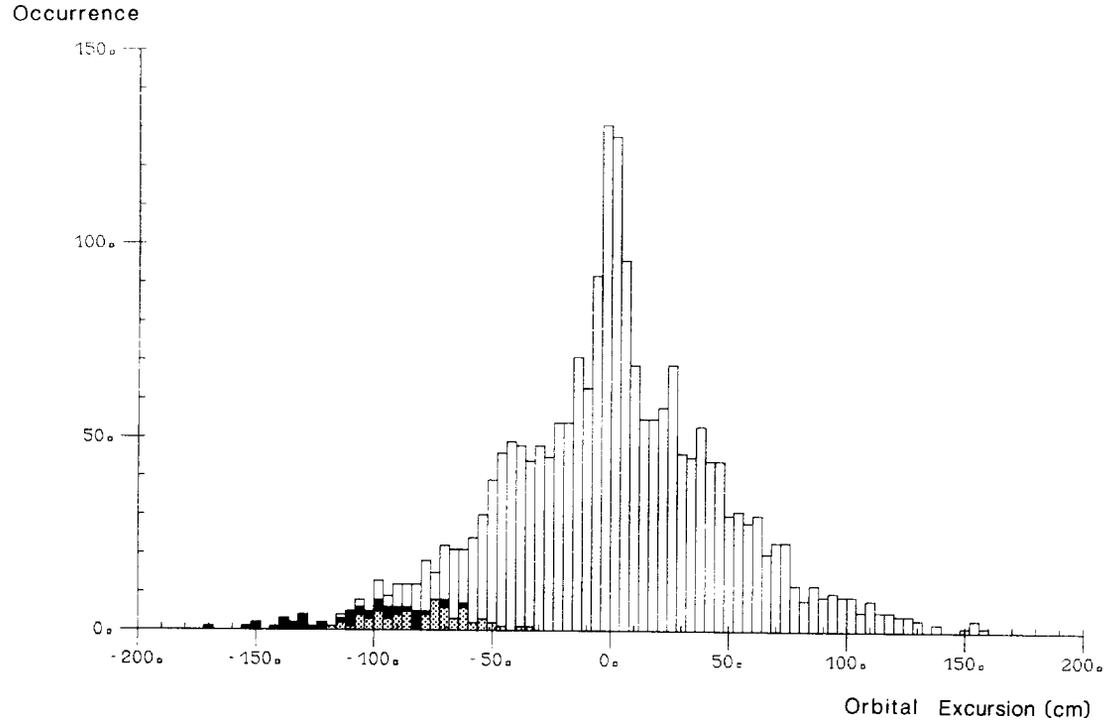

Fig 29: Histogram showing calculated orbital excursions for Runs 8 - 14, 1978. (Wave half cycles with double velocity maxima have been excluded). Shading is as in Fig 28.

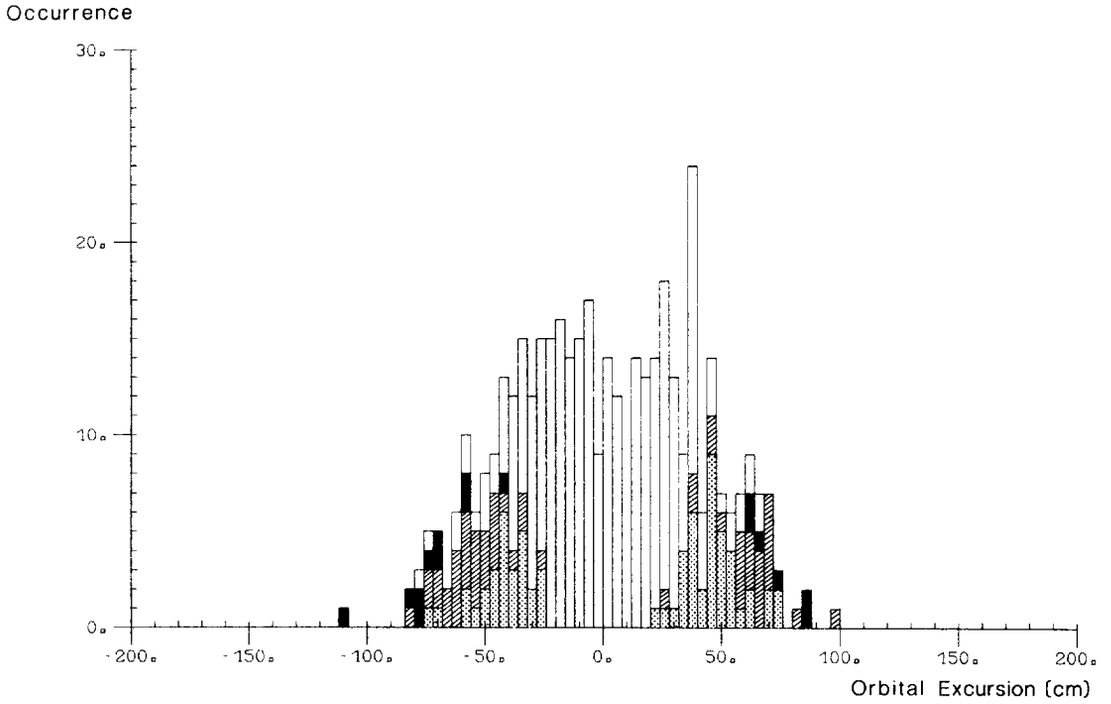

Fig 30: Histogram showing calculated orbital excursions for Run 12, 1980. (Wave half cycles with double velocity maxima have been excluded). Shading is as in Fig 26.

In order to gain a working understanding of the nature of the velocity field in separating flow over a rippled bed, a two-dimensional "standing vortex" model has been developed. This model, which is a simple extension of the single vortex pair model of Tunstall and Inman (1975), is based on methods of classical potential flow theory; the formulation is discussed by Davies (in prep). The present aim has been to use the model to calculate near bed velocities for that part of each wave half cycle in which the free stream velocity is near its maximum value, and in which a vortex is fully formed above the lee slope of each ripple. The flow has been assumed to be deep compared with a ripple wavelength, and the rippled bed to be of infinite horizontal extent. (In principle, the model is more appropriate for application to steady flows than it is to unsteady flows. However, its use in the unsteady case may be justified, up to a point, by previous laboratory results.) If the flow above an idealized naturally rippled bed is non-separating, the streamlines and the associated surface velocity components are as shown in Fig 31. For the typical natural ripple steepness in question (H_R/L_R = 0.15), the surface velocity at the crest is much enhanced compared with the free stream velocity, while the velocity in the trough is correspondingly diminished. Also, the convergences and divergences of the streamlines above the crests and troughs give way to an unperturbed uniform horizontal flow at about half a ripple wavelength above the mean bed level. Equivalent results for separating flow are shown in Fig 32, in which the position of the vortex above each lee slope has been specified in the model on the basis of previous laboratory work. Clearly, the streamlines and the surface velocities are fundamentally different from those for nonseparating flow. Apart from the very different implications for wave energy dissipation in the two cases, there are also different implications for sediment transport. In the nonseparating case, for which the orbital excursion may be supposed to be less than the ripple wavelength and for which the ripples are not in equilibrium with the prevailing flow, bed shear stresses are greatest in the region of the crests where the (tangential) surface velocities are greatest. It is not surprising, therefore, to find sediment motion occurring only in the vicinity of the crests and not in the troughs (Figs 24 and 25). By comparison, in the separating flow case, for which the orbital excursion is greater than the ripple wavelength and the ripples are in equilibrium with the outer flow, bed shear stresses are greatest on the lee slopes of the ripples and are directed towards the ripple crests. The fact that sediment is drawn towards the crests from both directions enables ripples to grow, at least until an equilibrium is achieved with the restoring influence of gravity on the ripple profiles. Further

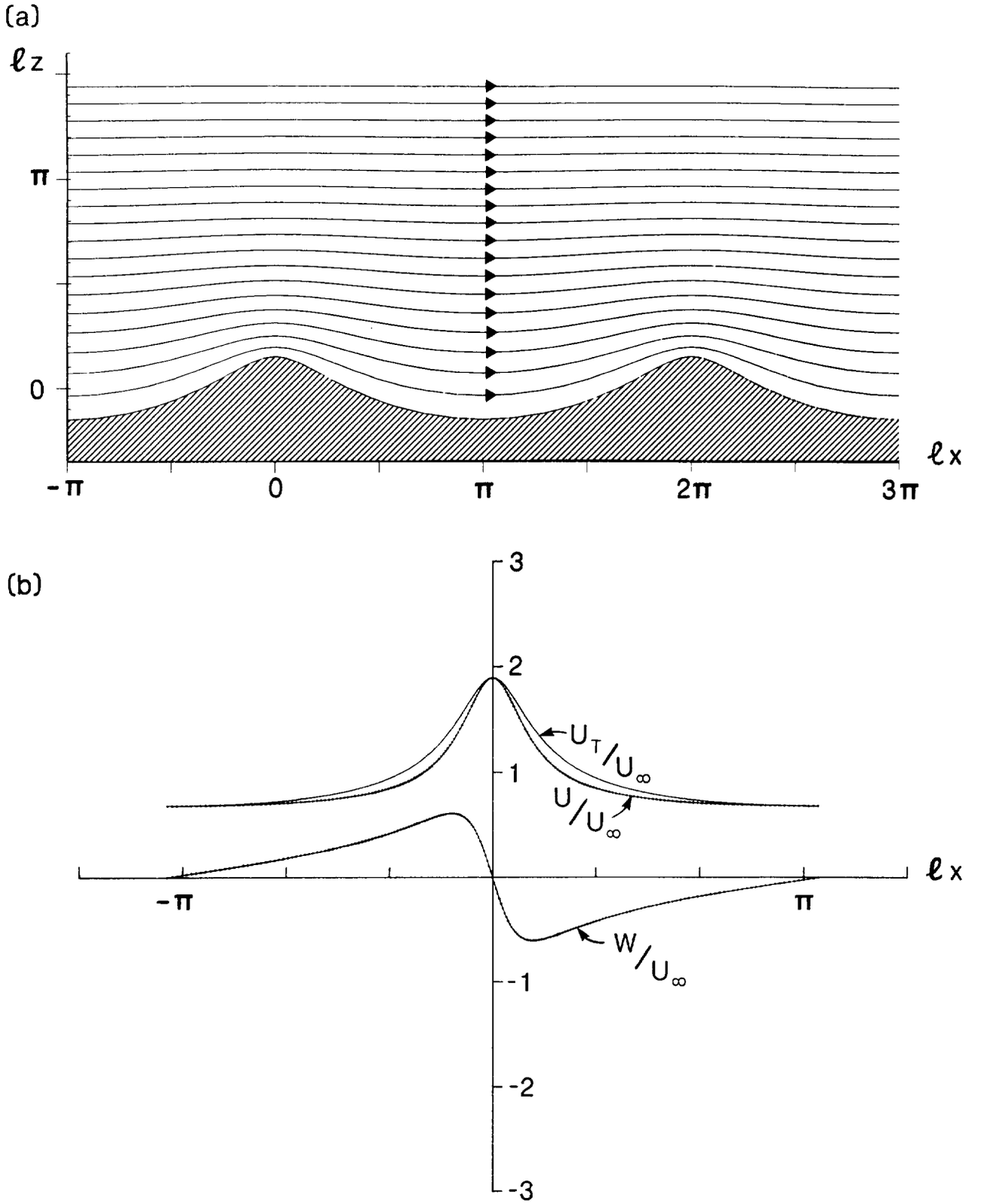

Fig 31: Nonseparating potential flow over ripples of steepness $H_R/L_R = 0.15$, ($1 = 2\pi/L_R$). Fig 31 (a) shows the streamlines, and 31 (b) the surface velocity components. The unperturbed horizontal velocity well above the bed (strictly, at infinity) is denoted by U_∞, and the tangential bed velocity is denoted by $U_T = \sqrt{\{U^2 + W^2\}}\,\mathrm{sgn}\,(U)$.

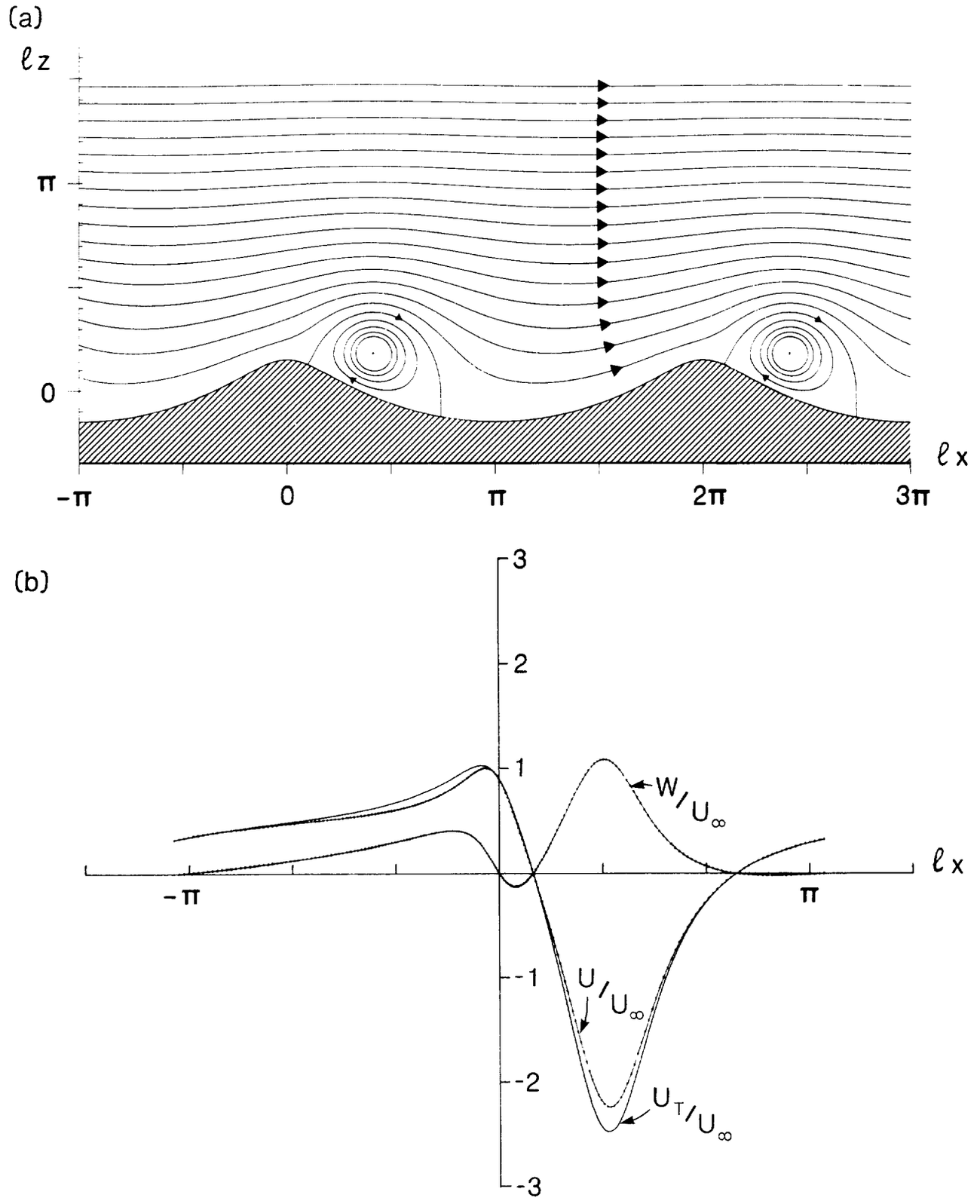

Fig 32: Separating potential flow over ripples of steepness $H_R/L_R = 0.15$.
Fig 32(a) shows the streamlines, and 32(b) the surface velocity components.
The notation is as for Fig 31.

obvious implications for sediment transport arise when the vortices are shed from the bed upon flow reversal. If the vortices are sediment laden, vortex shedding is a potent way in which sediment entrainment may occur. Vortex formation and shedding thus serves, firstly, to mobilize and entrain sediment; secondly, to stabilize ripple formations on the bed; and, thirdly, to give rise to high wave energy dissipation rates. Although it has not been possible to compare results such as those shown in Fig 32 with field measurements, the potential model appears to predict the important features of separating flow correctly, and the future development of this model holds out the prospect of an improved general understanding of near bed processes.

4. DISCUSSION AND CONCLUSIONS

The aim of this study has been not to further proliferate the choice of sediment transport formulae available to the engineer, but rather to clarify those aspects of application or interpretation, common to many of the existing formulae, which lead to difficulties when they are used in the sea. When these difficulties have been fully understood, it is hoped that the existing formulae can be used as successfully in the sea as they are in rivers. It is shown also that laboratory criteria for wave-induced sediment transport can be successfully applied in the sea provided that a rigorous approach is taken.

Accurate specification of the bed shear stress τ_0, which is usually obtained from the friction velocity u_*, is important because a small error in determining u_* leads to a large error in the predicted sediment transport rate. The latter is generally a complicated function of u_*, but for a given grain size and water depth, the function can be approximated over a small range of u_* by a power law. For conditions typical of the sea, the exponent of the power law is found to be in the range 3 to 7. Thus, for example, if a value of u_* which is 75% of the true value is used (as might occur for one of the reasons outlined below), the predicted transport rate would be under estimated by a factor of between 2.4 and 7.5.

Contributions to the topics identified at the heads of sections 2 and 3 have been made in the following areas:

i) If a near-bed velocity profile has been measured,a relatively good fit to the standard logarithmic form may often be obtained; however, a small amount of curvature may lead to the derived values of u_* and z_0 having large errors. The oscillatory nature of tidal flows has a marked effect on velocity profiles and shear stresses during a period from about 1 hour before, to 1 hour after, slack water. A detailed argument by Soulsby and Dyer (1981) showed that the assumption of a logarithmic form for velocity profile measurements made over a range of heights having a geometric mean height of 50 cm, in a semidiurnal tidal flow with a true peak $u_* = 3$ cm s^{-1} and a true $z_0 = 0.5$ cm, would lead to u_* and z_0 being overestimated by 20% and 83% respectively at 1 hour before slack water, and underestimated by 20% and 60% at 1 hour after slack water. However, during the period around slack water, the bed shear stress will often be below the threshold of motion for sand, so that inaccuracies in determining u_* then are not important for noncohesive sediment transport. Outside of this period the derivation of u_* and z_0 from measured currents, via either the logarithmic profile or the quadratic friction law, may be valid. The validity decreases with the height at which the current is measured, and the maximum acceptable height varies with the phase of the tide, being greatest at about peak current.

ii) Complications in determining u_* and z_0 also arise once sediment is in motion. This can be due to several causes: a) the ripple shape, and thus the bed geometry, may change (due principally to bedload transport) with time, causing tidal variations in z_0; b) saltation of grains enhances the momentum transfer from the flow to the bed, which is seen as an increase in z_0; c) suspended sediment produces a vertical density gradient which causes the velocity profile to deviate from its logarithmic form. These topics have been studied in three different field experiments, and also theoretically. It has proved difficult to draw simple conclusions which are compatible with all the evidence obtained, perhaps because the relative contributions of effects (a), (b) and (c) depend strongly on the exact experimental conditions, so we will simply list the results as they stand.

The theoretical treatment combined a number of standard expressions to produce an indication of the degree of stratification to be expected for a given grain diameter and bed shear stress. The resulting diagram (Fig 12) applies to the idealised case of steady uniform flow over an unrippled bed of a single grain size, and also, of course, relies on the standard expressions being accurate.

The positions of d_{50} and u_* at the time of peak current are marked on Fig 12 for the three field experiments. All of them lie in the zone in which the lower part of the profile is predicted to be stratified. The first field experiment, based on current measurements at 1.5 and 2.5 m above the bed, indicated that estimates of u_* and z_0 around the time of peak current were appreciably reduced from their expected values. It was hypothesised that this was due to sediment transport effects, but no sediment measurements were available to check this. In the second experiment it was found that the turbulent intensity decreased as the degree of stratification due to suspended sediment increased. This shows that the flow structure was modified by the suspended sediment, but velocity profiles were not measured on this occasion. The third experiment was designed specifically to investigate sediment-induced changes in u_* and z_0. However, the tidal variation observed in z_0 (a gradual increase through the tide) did not appear to correlate with any of the mechanisms (a) to (c) above, and might instead be attributable to other, nonsedimentary, causes. At a first glance this appears to contradict Fig 12, which predicts that stratification should modify the profile under these conditions. However, the theoretical work of Taylor and Dyer (1977) showed that the effect of sediment-induced stratification on z_0 is very sensitive to the parameter $b = w_s/ku_*$. The apparent value of z_0 is greater than or less than the unstratified value, depending on whether b is less than or greater than 1 respectively, and is equal to the unstratified value for the special case $b = 1$. This may explain the lack of z_0 variation observed in the third experiment, as the combination of grain size and u_* at that site, at the time of peak concentration, gave a value of $b = 0.95$.

To sum up, the evidence for the effect of sediment transport on the flow characteristics, based on our work and the previous literature, is not conclusive, and is probably very sensitive to the grain size and bed shear stress present. Values of u_* and z_0 obtained from velocity profiles at times when sediment is mobile should therefore be treated with caution.

iii) Ripple migration rates can give a lower bound to the bedload transport rate, but underestimate it by a factor of up to 2.5. With sandwaves, however, the migration rate may exceed the bedload transport rate when sediment is in suspension, but it is less than the <u>total</u> transport rate. Only if it is known that there is no transport across the troughs, is the migration rate equal to the sediment transport rate.

iv) Examinations of the bursting phenomenon and flux angle distribtuion have led to a more detailed understanding of the shear stress. The greater shear stress observed under a faster current or over a rougher bed results from an increase in the amplitude of the bursting events, while their spacing, size and type distribution remain roughly constant. The time between events, and their duration, both decrease with current speed. This has implications for sediment transport. The threshold of motion is usually quoted in terms of a time-mean value of τ_o, but this actually corresponds to isolated motions at peak values of the instantaneous shear stress. Thus if one kind of flow has a mean value of τ_o which is made up of short-lived, infrequent, large amplitude events, while another having the same mean τ_o is made up of long duration, more frequent, low amplitude events, the former may move sediment while the latter may not. This could contribute to the large scatter in measured thresholds observed in laboratory data. In the field it would mean that the same mean value of τ_o measured in accelerating and decelerating flows, in stratified and unstratified conditions, or on the upstream and downstream flanks of a sandwave, might cause differing sediment responses.

The relationship between the bursting phenomenon and sediment suspension is less strong than might be supposed, judging from the one rather poor data set analysed so far. In this, high sediment concentrations were most commonly associated with sweep events. A much better data set has now been obtained, which will be used to pursue this subject further.

v) Some progress has been made towards improving the specification of the reference concentration for suspended sediment. For a steady, uniform flow the balance of upward and downward sediment fluxes provides a differential equation, whose solution yields the concentration profile (eg the Rouse profile). A specified reference concentration is normally chosen as the boundary condition. However, a more physically meaningful boundary condition is that the upwards flux of sediment from the bed $(\overline{cw})_o$ should take a specified value, which will be a function of τ_o, properties of the sediment, and possibly the density stratification caused by the sediment. It has been shown theoretically that density stratification by the suspended sediment can be an important process. The experimental results showed that this leads to an appreciable reduction in the turbulent intensity, which provides a limit to the suspension process. The values of $\overline{cw}$ measured in the Taw experiment were too inconclusive to give any indication of the functional dependence of $(\overline{cw})_o$, and it would in any case be difficult to

estimate $(\overline{cw})_o$ from $\overline{cw}$ at one height. Measurements were made at more than one level in the 1982 Taw experiment, which when analysed may present a clearer picture.

vi) Field determinations of sediment threshold motion conditions, for irregular waves and mixed grain sizes, have been found to compare quite well with laboratory determinations for sinusoidal waves and a single grain size, the threshold criteria in both cases being in terms of free stream flow parameters.

vii) For wave induced flow above naturally rippled beds, calculations of bed shear stress amplitudes at the threshold of motion suggest that the total shear stress is about an order of magnitude larger than the skin friction. This may be contrasted with the situation in steady flow in which the total stress on a rippled bed is partitioned roughly equally between skin friction and form drag. The general significance of the partitioning of the stress is that, effectively, it is only the skin friction which acts directly on the grains on the bed surface. In fact, it has been confirmed in the present experiments in oscillatory flow, that there is fair agreement between the skin friction component of the total stress calculated for the field data, and the Shields' threshold stress from the laboratory.

viii) For motion due to waves, flow instability and, ultimately, vortex shedding above a rippled bed, appear to occur when the near bed orbital excursion is greater than the ripple wavelength. This well established laboratory result has been demonstrated on a wave-by-wave basis for the irregular waves measured in the field. It has been found in the present experiments also that equilibrium ripple wavelengths in irregular waves are rather less than the orbital excursions of those waves which moved sediment. An understanding of the relationship between the properties of surface waves, and the dimensions of the ripples which form on the bed, is important if wave energy dissipation rates, or sediment transport rates, are to be quantified. In the field, changes in wave conditions may give rise, after a time lag, to changes in ripple heights and wavelengths. The time lags involved are likely to be most significant during periods of diminishing wave activity; in fact, in the extreme case of a storm which dies away very rapidly, it is possible that a pattern of ripples generated by the highest storm waves may be fossilized on the bed. This is a more complicated situation than that which has usually been considered in laboratory work, and it calls for further study.

ix) An irrotational flow model has been developed to quantify some of the differences between separating and nonseparating flow above rippled beds, and to provide some insight into the near-bed processes of sediment motion and entrainment. The flow fields in the two cases are fundamentally different in respect of their implications both for sediment transport and for wave energy dissipation. In general, separating flow is likely to be associated with high waves above equilibrium rippled beds, and nonseparating flow with rather lower waves above nonequilibrium beds.

x) Two instruments have been developed: the Self Generated Noise probe, for bedload measurements, and the Sand Transport Probe for suspended load measurements. Field tests of the former show promise, especially for the larger grain sizes, and further development is actively in progress. The latter instrument can now be considered to be fully operational, and field tests have shown that in addition to the mean output calibrating well against pumped sample concentrations, the turbulent fluctuations in the concentration field are also well reproduced.

Because of the fundamental nature of the research, it also has applications to fields outside that of sediment transport. Thus the results obtained in the currents work make contributions to the fields of tidal dynamics, tidal prediction, storm surges, and dispersion of pollutants. Similarly the results obtained in the waves work contribute to the fields of wave energy dissipation, forces on offshore structures, and remote sensing of bottom topography.

Some work will continue to be done on the currents and waves topics separately, in particular on tightening up of areas where partial answers have already been obtained. However, the main thrust over the next few years will be in the field of sediment transport by surface waves superimposed on tidal currents. This is the most commonly occurring condition, and probably the most significant contributor to long-term sediment transport, in British coastal waters.

It is probable that engineers will never need to take account directly of many of the details investigated herein, but the basic conclusions drawn should help to reduce the degree of empiricism present in current predictions of sediment transport and ensure efficient and safe engineering practice.

ACKNOWLEDGEMENTS

We gratefully acknowledge the work of the IOS(T) instrumentation team, particularly Dr A P Salkield and Mr G P Le Good, in building, maintaining and operating the instruments; that of Ms H L King, Mrs B Wainwright and Mrs L Ellett in the data analysis; and that of Mr J Chappell in some of the theoretical aspects. We wish to thank the Director of the Marine Biological Association for permission to use R V Sarsia and R R S Frederick Russell, and the captain, officers and crew for their cooperation during the data collection in Start Bay; the Station Manager of the Central Electricity Generating Board's East Yelland Power Station for permission to work on their site, and the management and staff for their cooperation during the data collection in the River Taw; and Lady A Newmann for permission to work at Blackpool Sands.

APPENDIX

MEANINGS OF TERMS AND SYMBOLS USED

The terms used in the report may not be in common use in some branches of engineering. This appendix therefore acts as a glossary, by illustrating the usage and interrelations between the terms, in addition to listing the symbols used. Fuller accounts of the near-bottom properties of tidal currents are given by Bowden (1978) and Soulsby (1983); of surface waves by Smith (1977) and Davies (1983); and of sediment transport by Graf (1971) and Yalin (1977).

A.1 Terms used in describing the near-bottom properties of tidal currents

Tidal currents feel the frictional effects of the seabed within a boundary layer, occupying typically the bottom 20-80 m of the water column. In shallow water it may occupy the entire depth of water. The current speed varies with height from zero at the bed to a free-stream value at the top of the boundary layer, above which it is constant with height. In shallow water the current varies with height right up to the surface. Within the boundary layer the flow is turbulent, and the sum of the squares of the fluctuating turbulent velocity components determines the turbulent kinetic energy per unit mass of water, which is generally greatest near the bed and decreases upwards. The friction of the layers of water slipping over one another produces a shear stress which is almost entirely a turbulent process, and more or less synonomous with the turbulent Reynolds stress, $-\rho\overline{uw}$. It is zero at the top of the boundary layer (or at the water surface), and generally increases downwards towards the bed, where its value is the bed shear stress, τ_0, which is the frictional drag force acting on unit area of the bed. Another convenient quantity is the friction velocity, defined by $u_* = (\tau_0/\rho)^{\frac{1}{2}}$.

The bed shear stress can be measured in a number of ways. One of the simplest is to relate it to a current measurement at a single height, usually 100 cm, via the quadratic friction law

$$\tau_0 = \rho C_{100} U_{100}^2$$

where C_{100} is the drag coefficient referred to the current U_{100} at 1 m above the bed. Depth-averaged numerical models of a sea area utilise another form of the same law,

$$\tau_0 = \rho C_D \hat{U}^2,$$

where C_D is the drag coefficient referred to the depth-averaged current $\hat{U}$. Generally $C_D < C_{100}$. An alternative, more accurate, method is to measure the current at several heights in the bottom 2 m or so, where the logarithmic velocity profile,

$$U = \frac{u_*}{\kappa} \ln(z/z_0),$$

generally holds, from which u_*, and hence τ_0, is obtained. Von Karman's constant, κ, has the experimental value 0.40. The roughness length, z_0, is mathematically related to the drag coefficients, but has more general validity, as it is not height specific. Values of z_0, C_{100} and C_D depend on the nature of the seabed, being larger over rougher beds. They are independent of current speed at large values of the roughness Reynolds number u_*d/ν, for which the hydrodynamic roughness regime is rough turbulent, but vary with current speed otherwise. The peak tidal flow over a rippled sand bed is generally rough turbulent.

These simple expressions are only valid if the stability is near-neutral; that is, if the water density is homogeneous from bed to surface. The turbulence structure will be modified, and the bed shear stress and velocity profile altered, by density stratification due to vertical gradients of temperature, salinity or suspended sediment concentration. Where this occurs in the sea, the water is most commonly stably stratified, that is, the density increases downwards rather than upwards. A measure of the degree of statification is given by z/L, where L is the Monin-Obukhov length,

$$L = \frac{\rho u_*^3}{g\kappa\,\overline{\rho' w}},$$

and $\overline{\rho' w}$ represents the vertical flux of density. Positive values of L correspond to stable stratification, and $|z/L| < 0.03$ defines near-neutral stability.

The dominant tide in British waters has a semidiurnal period of 12 hr 25 min. Where the time-dependence of the tidal current is roughly sinusoidal, any day-to-day variation, due for example to meteorological effects, can be averaged out by extracting the semidiurnal tide by harmonic analysis. Near to coasts, however, the current may be very different to sinusoidal in form, and a more appropriate smoothing method is to divide the record into individual tides (High Slack Water to next HSW) and take an ensemble average (at each tidal phase) of several similar tides.

A.2 Terms used in describing the near-bottom properties of water waves

Many of the terms used in connection with tidal currents are also used in connection with wave-induced oscillations. The principal qualitative difference between the two cases is that,for surface wave frequencies, the oscillatory bottom boundary layer is generally very thin compared with the water depth. Boundary layer thicknesses are of the order of a few millimeters if the flow is laminar, and of the order of 10 cm if the flow is fully rough turbulent. Above the wave boundary layer (and in the absence of any turbulence generated by, for example, tidal currents or breaking waves at the free surface), the free stream flow comprises a nonturbulent layer in which little wave energy is dissipated. This essentially frictionless flow has been treated in the (idealized) theory of water wave motions as an irrotational flow.

Wave drag coefficients are defined in an analagous way to tidal drag coefficients. A commonly used drag coefficient, f_w, is defined by

$$\hat{\tau}_0 = \tfrac{1}{2}\rho f_w \hat{U}^2,$$

which is a relationship between the peak bed shear stress $\hat{\tau}_0$ in a sinusoidal wave half cycle and the peak velocity in the oscillatory free stream flow $\hat{U}$. By convention, a factor 1/2 appears in the drag law for waves, but not for currents. Values of the drag coefficient depend rather critically upon whether or not the bed is rippled and, if so, whether the flow remains everywhere attached to the bed (nonseparating or contouring flow) or whether vortices are formed above the lee slopes of the ripples (separating flow). The criterion which governs the onset of vortex formation is that the orbital excursion of the water particles in the free stream flow just above the bed should exceed the ripple wavelength; here the orbital excursion is the horizontal distance travelled by a water particle between consecutive instants when it is at rest (ie instants separated by an interval of one half of the wave period).

A.3 Terms used in describing sediment transport

The bed shear stress (due to either currents or waves) represents a drag force acting on the sediment of which the bed is made. A sandy bed acted on by currents or waves is often rippled; in this case some of the bed shear stress is associated with the form drag created by the pressure field around the ripples, and it is to all intents and purposes only the remaining skin friction which acts directly on the sediment grains . If the skin friction exceeds the threshold

stress, which depends on grain size in a way given, for example, by Shields' curve (see Graf, 1971) it will move the bed sediment. If the threshold is only just exceeded, the sediment grains roll and hop along the bed as bedload, while for larger stresses the sediment goes into suspension. An intermediate mode of motion, saltation, in which grains move in short hops across the bed, is important in the atmosphere but relatively unimportant in the sea. As far as bedload is concerned, the term incipient motion is used to refer to the sporadic movement of a few grains here and there on the bed, while the term general motion is used for the movement of grains over the entire bed surface. The variation of suspended sediment concentration with height is given in dimensionless form by, for example, the Rouse profile (see Graf, 1971); to use this in a practical situation it is necessary to re-dimensionalise it using a reference concentration, which will be a function of grain size and τ_0.

A.4 Notation

Symbol	Meaning
b	exponent of Rouse concentration profile, $b = w_s/\kappa u_*$.
C_D	drag coefficient used with depth-averaged current velocity.
C_{100}	drag coefficient used with current velocity 100 cm off the bottom.
C	concentration of suspended sediment (dry mass per unit volume).
c	fluctuating part of C.
d	grain diameter.
$d_{10}(d_{50}, d_{90})$	the grain diameter for which 10% (50%, 90%) of the mass of a mixed sediment is finer.
$E_{\alpha\alpha}(k)$	energy spectrum of variable α.
f	frequency.
f_w	wave friction factor of Jonsson (1966).
g	acceleration due to gravity.
H_R	ripple height.
h	water depth.
h_{log}	height of logarithmic layer.
k	wavenumber of turbulent fluctuations, converted from frequency via Taylor's hypothesis, $k = 2\pi f/\bar{U}$.
L	Monin-Obukhov length.
L_R	ripple wavelength.
l	ripple wavenumber = $2\pi/L_R$.
S	area of seabed associated with one roughness element.
s	frontal area of roughness element.
ΔT	zero crossing half-period of an irregular wave half cycle.
U	x-component of velocity.
u	fluctuating part of U.
u_*	friction velocity.
u_{*c}	threshold friction velocity for sediment movement.
V	y-component of velocity.
v	fluctuating part of V.
w	fluctuating part of vertical velocity component, positive upwards.
w_s	grain settling velocity, positive downwards.

x,y	horizontal Cartesian coordinate axes, orientation depends on application.
z	vertical Cartesian coordinate axis with origin at bed surface and positive upwards.
z_0	roughness length.
α	any variable.
κ	von Karman's constant ($\simeq 0.40$).
λ	wavelength of turbulent fluctuations, $\lambda = 2\pi/k$.
ρ	density of water.
ρ'	fluctuating part of ρ.
τ	shear stress.
τ_0	bed shear stress.
$\bar{\alpha}$	mean of variable α over a suitable period, typically 10 minutes.
$\hat{\alpha}$	amplitude of a sinusoidally varying variable α. (Or the peak value of α in an irregular wave half cycle).
$\mathrm{sgn}(\alpha)$	+1 or -1 according to the sign of α.
$\ln(\alpha)$	natural logarithm of α.

Subscripts T and ∞ are used to denote velocities in the irrotational flow model: U_T denotes the tangential component of bed velocity, defined by $U_T = \sqrt{u^2 + w^2}\ \mathrm{sgn}(u)$, and U_∞ denotes the unperturbed horizontal velocity well above the rippled bed (strictly, at infinity).

REFERENCES

BAGNOLD, R A, 1946. Motion of waves in shallow water. Interaction between waves and sand bottoms. Proceedings of the Royal Society of London, Series A, 187, 1-18.

BAGNOLD, R A, 1980. An empirical correlation of bedload transport rates in flumes and natural rivers. Proceedings of the Royal Society of London, Series A 372, 453-473.

BOWDEN, K F, 1978. Physical problems of the benthic boundary layer. Geophysical Surveys, 3, 255-296.

COMTE-BELLOT, G, SABOT, J and SALEH, I, 1978. Detection of intermittent events maintaining Reynolds stress. Pp 213-229 in Proceedings 1978 Dynamic Flow Conference on Dynamic Measurements in Unsteady Flows, held in Marseilles and Baltimore. Dynamic Flow Conference, Skovlunde, Denmark, 1040 pp.

DAVIES, A G, 1979. The potential flow over ripples on the seabed. Journal of Marine Research, 37, 4, 743-759.

DAVIES, A G, 1980. Field observations of the threshold of sand motion in a transitional wave boundary layer. Coastal Engineering, 4, 23-46.

DAVIES, A G, 1982. On the interaction between surface waves and undulations on the seabed. Journal of Marine Research, 40, 2, 331-368.

DAVIES, A G, 1983. Wave interactions with rippled sand beds. Ch 1 of Physical Oceanography of Coastal and Shelf Seas. Edited by B Johns, Amsterdam: Elsevier (in press).

DAVIES, A G, FREDERIKSEN, N A and WILKINSON, R H, 1977. The movement of non-cohesive sediment by surface water waves. Part 2: Experimental Study. Institute of Oceanographic Sciences Report No 46, 80 pp.

DAVIES, A G and WILKINSON, R H, 1979. Sediment motion caused by surface water waves. Pp 1577-1595 in Proceedings of the 16th Coastal Engineering Conference, Hamburg. Volume 2. New York: American Society of Civil Engineers.

DAWSON, G P, JOHNS, B and SOULSBY, R L, 1983. A numerical model of shallow flow over topography. Ch 6 of Physical Oceanography of Coastal and Shelf Seas. Edited by B Johns. Amsterdam: Elsevier (in press).

DYER, K R, 1980. Velocity profiles over a rippled bed and the threshold of movement of sand. Estuarine and Coastal Marine Science, 10, 181-199.

EINSTEIN, H A, 1950. The bedload function for sediment transportation in open channel flows. United States Department of Agriculture, Soil Conservation Service, Technical Bulletin No 1026, 78 pp.

GILLETTE, D A and PORCH, W M, 1978. The role of fluctuations of vertical and horizontal wind and particle concentration in the deposition of dust suspended by wind. Journal of Geophysical Research, 83, 409-414.

GORDON, C M, 1974. Intermittent momentum transport in a geophysical boundary layer. Nature, 248, 392-394.

GRAF, W H, 1971. Hydraulics of sediment transport. New York: McGraw-Hill, 513 pp.

GRANT, W D and MADSEN, O S, 1982. Movable bed roughness in unsteady oscillatory flow. Journal of Geophysical Research, 87, C1, 469-481.

GRASS, A J, 1971. Structural features of turbulent flow over smooth and rough boundaries. Journal of Fluid Mechanics, 50, 233-255.

GRASS, A J, 1976. Transport of fine sand on a flat bed: turbulence and suspension mechanics. Pp 33-34 in: Euromech 48, Proceedings of the Colloquium on Transport, Erosion and Deposition in Turbulent Streams, held Copenhagen Institute of Hydrodynamics and Hydraulic Engineering, Lyngby, 57 pp.

HEATHERSHAW, A D, 1974. "Bursting" phenomena in the sea. Nature, 248, 394-395.

HEATHERSHAW, A D, 1981. Comparisons of measured and predicted sediment transport rates in tidal currents. Marine Geology, 42, 75-104.

HICKS, B B and DYER, A J, 1972. The spectral density technique for the determination of eddy fluxes. Quarterly Journal of the Royal Meteorological Society, 98, 838-844.

JONSSON, I G, 1966. Wave boundary layers and friction factors. Pp 127-148 in Proceedings of the 10th Coastal Engineering Conference, Tokyo. New York: American Society of Civil Engineers.

KAMPHUIS, J W, 1975. Friction factor under oscillatory waves. Proceedings of the American Society of Civil Engineers. Journal of the Waterways, Port, Coastal and Ocean Division, 101, No WW2, 135-144.

KOMAR, P D and MILLER, M C, 1975. Sediment threshold under oscillatory waves. Pp 756-775 in Proceedings of the 14th Coastal Engineering Conference, Copenhagen. New York: American Society of Civil Engineers.

LETTAU, H, 1969. Note on aerodynamic roughness parameter estimation on the basis of roughness element description. Journal of Applied Meteorology, 8, 828-832.

MANOHAR, M, 1955. Mechanics of bottom sediment movement due to wave action. US Army, Corps of Engineers, Beach Erosion Board. Technical Memorandum No 75, 121 pp.

MARKS, A J, WHELLOCK, J L and SALKIELD, A P, 1981. A monitor for measuring the movement of marine bedforms. Pp 19-26 in Proceedings of IERE Conference on Electronics for Ocean Technology held in Birmingham. London: Institution of Electronic and Radio Engineers, 348 pp.

McBEAN, G A, 1974. The turbulent transfer mechanism: a time domain analysis. Quarterly Journal of the Royal Meteorological Society, 100, 53-66

NIELSEN, P, 1979. Some basic concepts of wave sediment transport. Technical University of Denmark, Institute of Hydrodynamics and Hydraulic Engineering. Series Paper No 20, 160 pp.

OWEN, P R, 1964. Saltation of uniform grains in air. Journal of Fluid Mechanics, 20, 225-242.

SALKIELD, A P, LE GOOD, G P and SOULSBY, R L, 1981. An impact sensor for measuring suspended sand concentration. Pp 36-47 in Proceedings of IERE Conference on Electronics for Ocean Technology, held in Birmingham. London: Institution of Electronic and Radio Engineers, 348 pp.

SLEATH, J F A, 1975. Transition in oscillatory flow over rippled beds. Proceedings of the Institution of Civil Engineers, 59, 2, 309-322.

SLEATH, J F A, 1976. On rolling-grain ripples. Journal of Hydraulic Research, 14, 1, 69-81.

SMITH, J D, 1977. Modeling of sediment transport on continental shelves. Pp 539-578 in The Sea, Vol 6. Edited by E D Goldberg, I N McCave, J J O'Brien, J H Steele. New York: Wiley - Interscience, 1084 pp.

SMITH, J D and McLEAN, S R, 1977. Spatially averaged flow over a wavy surface. Journal of Geophysical Research, 82, 1735-1746.

SOULSBY, R L, 1978. Personal communication.

SOULSBY, R L, 1983. The bottom boundary layer of shelf seas. Ch 5 of Physical Oceanography of Coastal and Shelf Seas. Edited by B Johns. Amsterdam: Elsevier (in press).

SOULSBY, R L and DYER, K R, 1981. The form of the near-bed velocity profile in a tidally accelerating flow. Journal of Geophysical Research, 86, 8067-8074.

TAYLOR, P A, and DYER, K R, 1977. Theoretical models of flow near the bed and their implications for sediment transport. Pp 579-601 in The Sea, Vol 6. Edited by E D Goldberg, I N McCave, J J O'Brien, J H Steele. New York: Wiley - Interscience, 1084 pp.

TUNSTALL, E B and INMAN, D L, 1975. Vortex generation by oscillatory flow over rippled surfaces. Journal of Geophysical Research, 80, 24, 3475-3484.

WILKINSON, R H, 1983. A method for evaluating statistical errors associated with logarithmic velocity profiles. Geo-Marine Letters (in press).

WILKINSON, R H, SALKIELD, A P and MOORE, E J, 1983. Photogrammetry in sediment transport studies. In Underwater Photography for Scientists. Edited by D George. Oxford: Oxford University Press (in press).

YALIN, M S, 1977. Mechanics of sediment transport (2nd edition). Oxford; Pergamon, 298 pp.